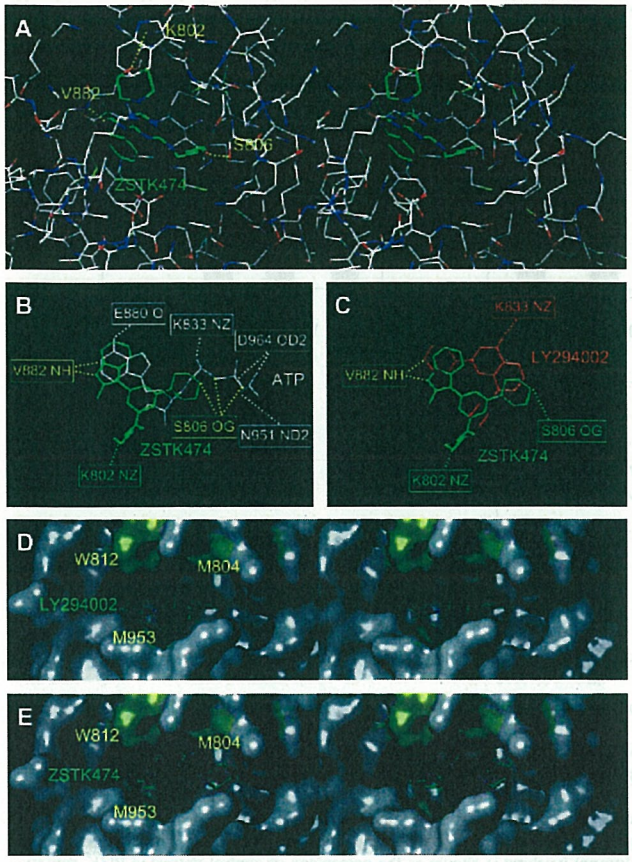

Fig. 4. Molecular modeling of the PI3K–ZSTK474 complex. A) Stereo view of the model structure of the PI3K–ZSTK474 complex. Putative hydrogen bonds = **yellow dashed lines.** Carbon atoms of PI3K = **white**; nitrogens = **blue**; oxygens = **red.** B and C) Binding modes in the PI3K active site. B) Comparison of ZSTK474 and ATP. ZSTK474 = **green**; ATP = **white.** C) Comparison of ZSTK474 and LY294002. ZSTK474 = **green**; LY294002 = **red.** D and E) Stereoview of the interactions between PI3K amino acid residues (M804, W812, and M953) and LY204002 or ZSTK474. D) LY294002 and PI3K. Amino acid residues = **yellow**; LY294002 = **green.** E) ZSTK474 and PI3K. Amino acid residues = **yellow**; ZSTK474 = **green.**

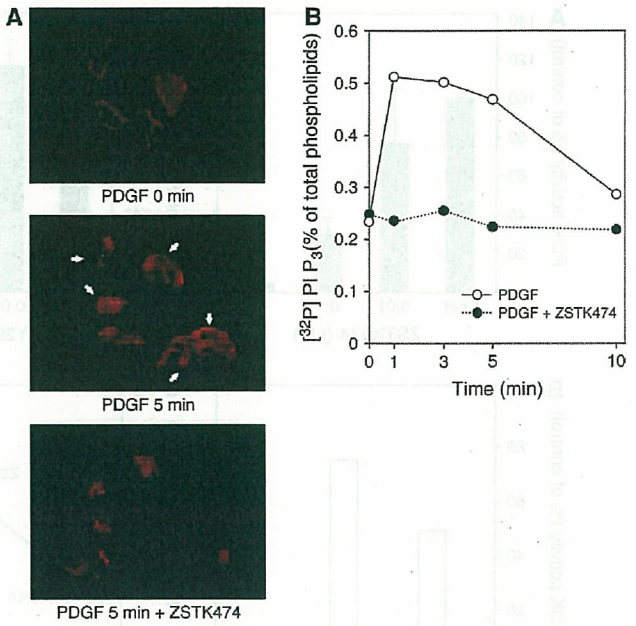

Fig. 5. Effect of ZSTK474 on membrane ruffling and the formation of phosphatidylinositol-3,4,5-trisphosphate (PIP_3). A) Inhibition of membrane ruffling in murine embryonic fibroblasts (MEFs) by ZSTK474. MEFs were treated with or without 1 μM ZSTK474 for 15 minutes and then stimulated with platelet-derived growth factor (10 ng/mL) for 5 minutes. Cells were then fixed and stained for filamentous actin with tetramethylrhodamine isothiocyanate–conjugated phalloidin (**red**). **Arrows** indicate cells with membrane ruffling. B) Inhibition of PIP_3 formation by ZSTK474. MEFs were labeled with [^{32}P]orthophosphate (0.1 mCi/mL) for 4 hours, treated with or without 1 μM ZSTK474 for 15 minutes, and then stimulated with platelet-derived growth factor (10 ng/mL) as indicated. Radioactivity in the total phospholipids and in PIP_3 was determined with a bioimaging analyzer. Data are the percentage of radioactive PIP_3 as a function of radioactivity in total lipids.

corresponding portion of the ATP-binding pocket of other protein kinases *(44)*. In our models, this space was occupied by the bulky 8-phenyl group of LY294002 (Fig. 4, D), as previously indicated by Walker et al. *(44)*, or by the triazine and morpholino groups of ZSTK474 (Fig. 4, E).

Inhibition of Membrane Ruffling by ZSTK474

It is widely accepted that membrane ruffling is regulated by PI3K by means of a pathway that is independent of Akt, a serine/threonine protein kinase. We examined ZSTK474 for its effect on membrane ruffling induced by platelet-derived growth factor in murine embryonic fibroblast cells. We found that membrane ruffling was induced 5 minutes after platelet-derived growth factor was added to the cultures (Fig. 5, A). When cells were incubated for 15 minutes with 1 μM ZSTK474 before the addition of platelet-derived growth factor, both membrane ruffling and the formation of PIP_3, a measure of PI3K activity, were blocked (Fig. 5, B). Thus, ZSTK474 appears to inhibit PI3K activity and also to block membrane ruffling.

Effects of ZSTK474 on Apoptosis and Cell Cycle

Because PI3K and its downstream components appear to mediate antiapoptotic signals, we examined the effect of ZSTK474 on the induction of apoptosis. At 10 μM, a higher concentration than its GI_{50}, ZSTK474 induced apoptosis in OVCAR3 cells (Fig. 6, A and B). However, 10 μM ZSTK474 did not induce apoptosis in A549 cells but instead mediated complete G_1-phase arrest (Fig. 6, C). Therefore, it appears that induction of apoptosis by ZSTK474 is a weak and cell type-dependent event. Here the induction of G_1-phase arrest by ZSTK474 might lead to the inhibition of tumor growth in vivo, which was indeed observed in the animal experiments with A549 below.

Inhibition of Akt Phosphorylation and Downstream Signaling by ZSTK474

The time course of ZSTK474-mediated inhibition of the phosphorylation of Akt, one of the major targets of PI3K, and inhibition of other downstream signaling components was examined in A549 cells by immunoblotting. Treatment with 0.5 μM ZSTK474 decreased the level of phosphorylated Akt (Ser-473) within 5 minutes without altering overall Akt protein levels and then decreased the level of phosphorylated GSK-3β (Ser-9) and of cyclin D1 protein expression within 30 minutes (Fig. 7, A). We next investigated the effect of various concentrations of ZSTK474

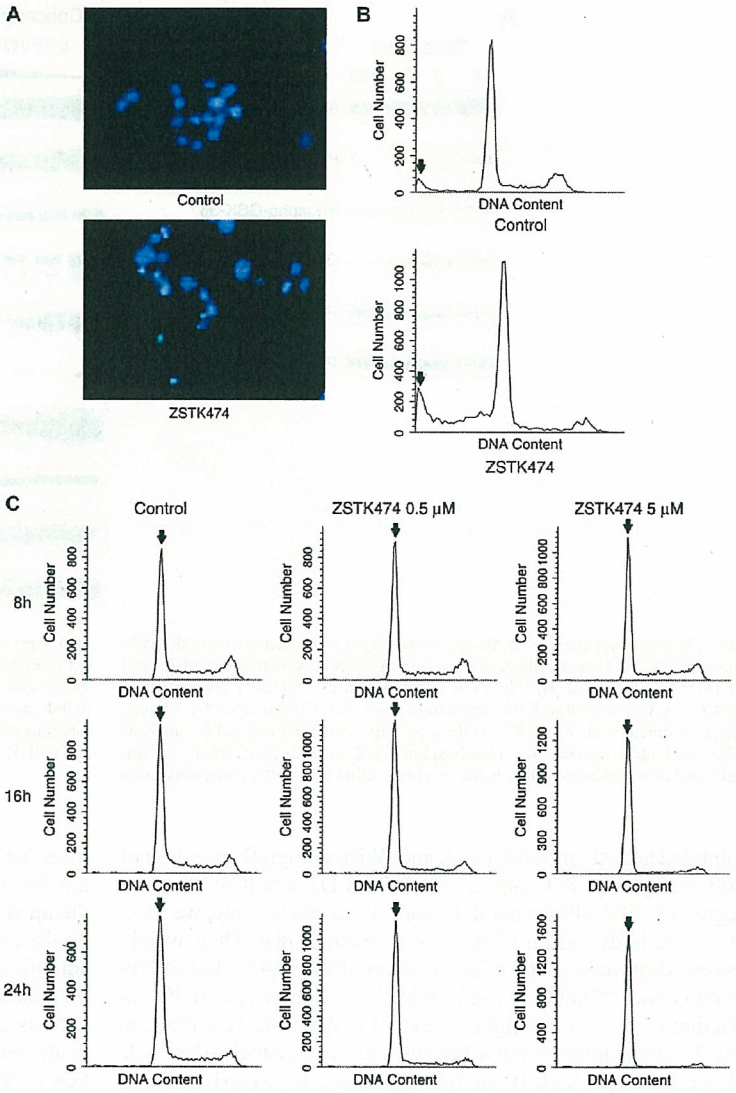

Fig. 6. Effects of ZSTK474 on apoptosis and cell cycle. A) Apoptosis assessed by chromatin condensation. OVCAR3 cells were cultured in RPMI 1640 medium supplemented with 5% fetal bovine serum for 24 hours and then cultured for 48 hours with or without 10 μM ZSTK474. Cells were stained with Hoechst 33342 and examined by fluorescence microscopy. Morphologic changes induced by ZSTK474, such as the condensation of chromatin, were indicative of apoptosis. B) Apoptosis as assessed by flow cytometry. OVCAR3 cells cultured under the same conditions as in **panel A** were harvested, washed with ice-cold phosphate-buffered saline (PBS), and fixed in 70% ethanol. Cells were then washed twice with ice-cold PBS again, treated with RNase A (500 μg/mL, Sigma) at 37 °C for 1 hour, and stained with propidium iodide (25 μg/mL, Sigma). The DNA content of the cells was analyzed with a flow cytometer (FACScalibur, Becton Dickinson). When exposed to ZSTK474, the sub-G_1 peak increased, indicating that ZSTK474 induced apoptosis. **Arrows** indicate the sub-G1 peaks. C) Cell cycle analysis as assessed by flow cytometry. A549 cells were exposed to 0.5 or 5 μM ZSTK474 for 8, 16, or 24 hours. The DNA content of the cells was determined by flow cytometry as described above. When exposed to ZSTK474, the cell population in G_1 phase increased time dependently, indicating that ZSTK474 blocked the cell cycle at the G_1 phase. **Arrows** indicate the G_1 peaks.

from 0 to 2.0 μM on the levels of downstream signaling components in the Akt pathway. ZSTK474 inhibited the phosphorylation of forkhead in rhabdomyosarcoma-like 1 (FKHRL1) on Thr-32, forkhead in rhabdomyosarcoma (FKHR) on Thr-24, tuberous sclerosis complex 2 (TSC-2) on Ser-1462, mammalian target of rapamycin (mTOR) on Ser-2448, and p70 ribosomal protein S6 kinase (p70S6K) on Thr-389 and decreased the expression of cyclin D1 protein in a dose–dependent manner (Fig. 7, B). In contrast, phosphorylation of extracellular signal-regulated kinases (ERK1/2) and mitogen-activated protein kinase/extracellular signal–regulated kinase kinases (MEK1/2) were not inhibited by ZSTK474, suggesting that ZSTK474 did not inhibit the RAS–ERK pathway (Fig. 7, A and B). Thus ZSTK474 also appears to act through the Akt pathway.

Antitumor Efficacy of ZSTK474 In Vivo

We evaluated the antitumor activity and toxicity of ZSTK474 by use of a mouse cancer model and three human cancer xenograft models. When administered orally for 2 weeks, ZSTK474 inhibited the growth of subcutaneously implanted mouse B16F10 melanoma tumors in a dose-dependent manner. Almost complete tumor growth inhibition (i.e., tumor regression) was observed at higher dosages. Administration of ZSTK474 at 100, 200, or 400 mg/kg produced tumor regression of 28.5% (95% CI = 21.4% to 35.7%), 7.1% (95% CI = 2.7% to 11.5%), or 4.9% (95% CI = 3.2% to 6.5%) on day 14, respectively. This growth inhibition was superior to that of the four major anticancer drugs examined—irinotecan, cisplatin, doxorubicin, and 5-fluorouracil (each administered at their respective maximum tolerable doses). Tumor regression in mice of treated with irinotecan, cisplatin, doxorubicin, or 5-fluorouracil was 96.0% (95% CI = 63.5% to 128.4%), 35.7% (95% CI = 28.6% to 42.9%), 24.0% (95% CI = 16.4% to 31.5%), or 68.3% (95% CI = 21.4% to 115.3%) on day 14, respectively (Fig. 8, A). Moreover, the myelosuppression induced by ZSTK474 at 400 mg/kg was marginal (Fig. 8, B).

We then examined the antitumor activity of ZSTK474 against A549, PC-3, and WiDr human xenografts, which originated from a non–small-cell lung cancer, a prostate cancer, and a colon cancer, respectively. Chronic oral administration of ZSTK474 completely

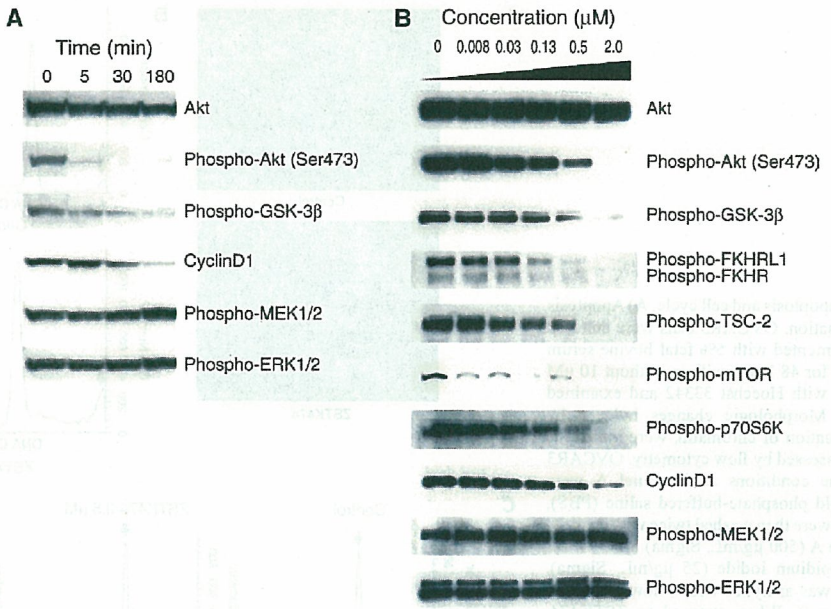

Fig. 7. Immunoblot analysis of Akt and downstream components in the Akt pathway in ZSTK474-treated cells. A) Time course. A549 cells were treated with 0.5 μM ZSTK474 as indicated. B) Inhibition as a function of ZSTK474 concentration. A549 cells were treated with the concentration of ZSTK474 indicated for 3 hours. After treatment with ZSTK474, cells were harvested for immunoblot analysis with antibodies specific for nonphosphorylated or phosphorylated proteins indicated of Akt phosphorylation, the level of cyclin D1, and the phosphorylation of downstream components, including glycogen synthase kinase 3β (GSK-3β), extracellular signal–regulated kinases (ERK1/2), mitogen-activated protein kinase/extracellular signal–regulated kinase kinases (MEK1/2), forkhead in rhabdomyosarcoma-like 1 (FKHRL1), forkhead in rhabdomyosarcoma (FKHR), tuberous sclerosis complex 2 (TSC-2), mammalian target of rapamycin (mTOR), and p70 ribosomal protein S6 kinase (p70S6K).

inhibited growth of A549, PC-3, and WiDr xenografts at a dose of 400 mg/kg (Fig. 8, C [upper panels] and D), and it induced the regression of A549 xenograft tumors. To assess toxicity, we measured the body weight of the tumor-bearing mice. Their weight was slightly reduced by administration of ZSTK474, but the reduction was tolerable (no reduction, 17% reduction, and 3% reduction of the day 0 weight on day 14 in A549-bearing mice, in PC-3-bearing mice, in WiDr-bearing mice, respectively) (Fig. 8, C [lower panels]). Dermal toxicity has been reported when LY294002 administered to nude mice *(46)*. However, we observed no dermal toxicity with ZSTK474 even after more than 28 days, as shown in Fig. 8, D. Furthermore, chronic oral administration of ZSTK474 at a higher dose (800 mg/kg) over 4 weeks again reduced body weight within a tolerable range (14% reduction of the day 0 weight on day 28), without toxic effects in critical organs. Thus ZSTK474 appeared to have good therapeutic efficacy in vivo.

Inhibition of the Phosphorylation of Akt by ZSTK474 In Vivo

To confirm that ZSTK474 inhibits the PI3K pathway in vivo, the phosphorylation status of Akt in the subcutaneous A549 tumor tissue was immunohistochemically determined by an anti-Akt antibody specific for phosphorylation at Akt amino acid residue Ser-473. We found that administration of ZSTK474 reduced the level of Akt phosphorylation in tumor tissue (Fig. 8, E).

Discussion

In this study, we demonstrated that a new compound, ZSTK474, is a potent inhibitor of PI3K that differs structurally from the well-known PI3K inhibitors LY294002 and wortmannin. We also demonstrated that orally administered ZSTK474 has therapeutic efficacy against human cancer xenografts in mice. To the best of our knowledge, this is the first report of an orally administered PI3K inhibitor that has strong antitumor activity without severe toxicity in vivo. The PI3K pathway is activated in various cancer types, and therefore PI3K is a promising therapeutic target of cancer *(3,4,21)*. Thus ZSTK474 appears to be a new anticancer drug candidate targeting PI3K.

From a methodology viewpoint, another novelty of this study is our use of an information-intensive approach, COMPARE analysis, to identify the target of ZSTK474. The COMPARE analysis predicted that the target of ZSTK474 was PI3K, which was later confirmed by direct inhibition of PI3K activity with ZSTK474. We have previously identified the targets of new compounds MS-247 *(26)* and FJ5002 *(47)* as topoisomerase I/II and telomerase, respectively, by using COMPARE analysis. This study further confirms that the COMPARE analysis is a powerful tool that can predict the molecular targets of new compounds.

Molecular modeling of the PI3K–ZSTK474 complex indicated that ZSTK474 could bind to the ATP-binding pocket of PI3K through three hydrogen bonds, which is a finding consistent with the ZSTK474-mediated inhibition of PI3K being reversible. Because ZSTK474 formed three hydrogen bonds with PI3K, instead of the two hydrogen bonds formed between LY294002 and PI3K, ZSTK474 appears to be a stronger competitor for the ATP-binding pocket of PI3K than LY294002. Indeed, the PI3K inhibitory activity of ZSTK474 was approximately 20-fold stronger than that of LY294002. Another important feature of ZSTK474 is its high specificity for PI3K. When tested at 30 μM, ZSTK474 did not inhibit the activity of 139 other

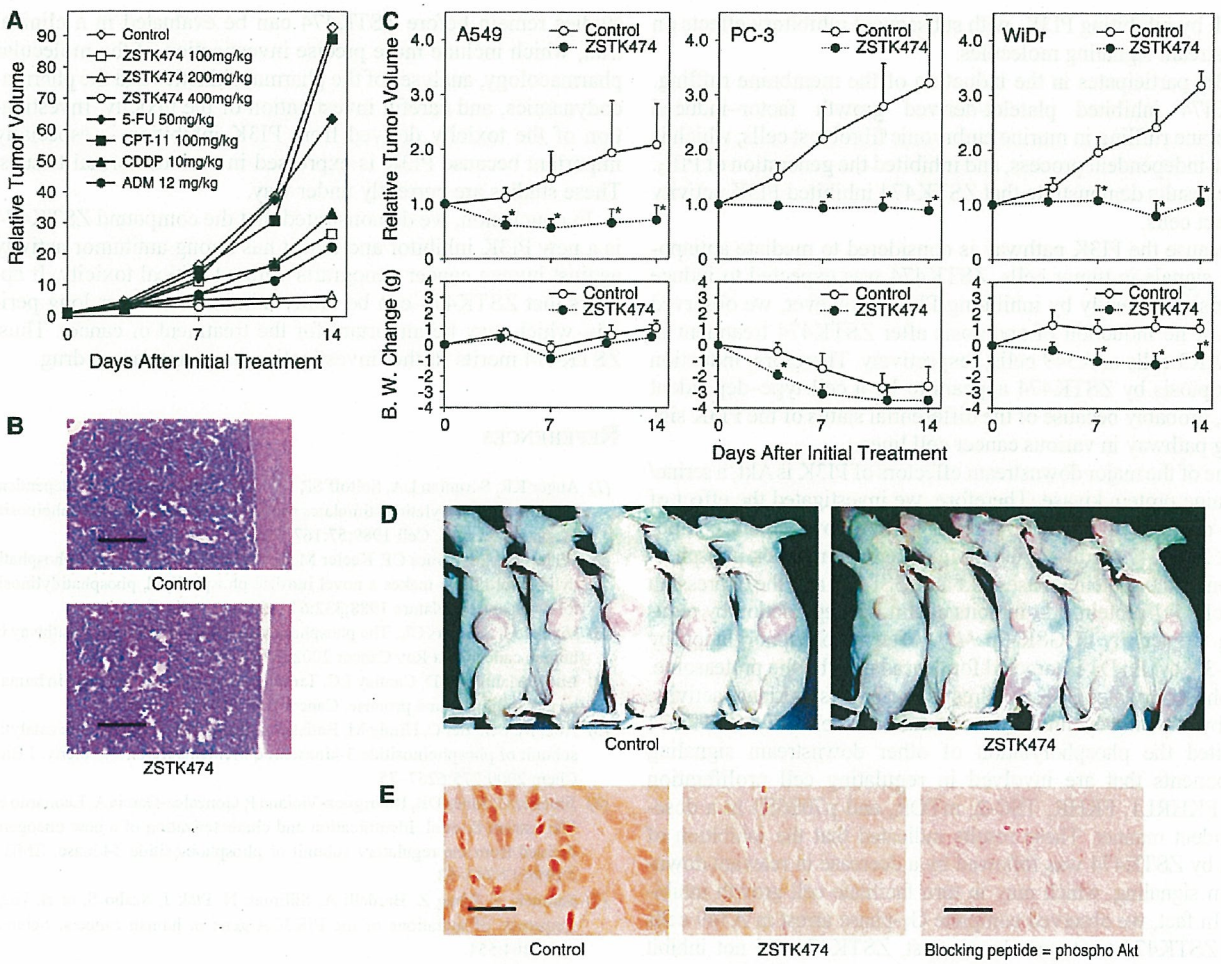

Fig. 8. Antitumor activity of ZSTK474. **A)** Antitumor activity of ZSTK474 against mouse B16F10 melanomas. Fifty-six BDF_1 mice were each subcutaneously injected with 5×10^5 B16F10 melanoma tumor cells. Seven days after inoculation, the administration of the drugs, as indicated, began (day 0). ZSTK474 was orally administered daily from days 0 to 13. Reference drugs were irinotecan (CPT-11), cisplatin (CDDP), doxorubicin (ADM), and 5-fluorouracil (5-FU). Each reference drug was administered intravenously from day 0 at the maximum tolerable dose by use of the following optimal schedules: CPT-11 at 100 mg/kg administered three times on days 0, 3, and 7; CDDP at 10 mg/kg once on day 0; ADM at 12 mg/kg once on day 0; and 5-FU at 50 mg/kg three times on days 0, 3, and 7. Each data point is the average of data from seven mice. **B)** Hematoxylin–eosin staining of femur bone marrow sections from BDF_1 mice bearing B16F10 melanomas 14 days after inoculation of tumor cells. ZSTK474 at 400 mg/kg was orally administered daily from days 0 to13. **Scale bar** = 100 μm. **C)** ZSTK474 and tumor growth and body weight in nude mice bearing human cancer xenografts. Forty-five nude mice were subcutaneously inoculated with a tumor fragment of 3 mm × 3 mm × 3 mm from the subcutaneous tumor developed in nude mice. When tumors reached a volume of 100–300 mm^3, animals were divided randomly into test groups, each with five mice (day 0). ZSTK474 (400 mg/kg) was orally administered daily from day 0 to 13 except for days 3 and 10. Data are the means of data from five mice. **Error bar** = the upper 95% confidence interval. *P = .009, two-sided Mann–Whitney U test, compared with respective control. **D)** WiDr xenograft growth inhibition after administration of ZSTK474. ZSTK474 at 400 mg/kg was orally administered daily from days 0 to 26, except for days 6, 13, and 20. The mice were photographed on day 28. Other experimental conditions were the same as described above. **E)** ZSTK474 and Akt phosphorylation in nude mice bearing A549 human non–small-cell lung cancer xenografts. When the volume of tumors reached 100–300 mm^3, ZSTK474 at 400 mg/kg was orally administered once. Mice were killed 4 hours after ZSTK474 administration, and excised tumors were analyzed by immunohistochemistry for the expression of phosphorylated Akt (Ser-473). Phosphorylated Akt (Ser-473) blocking peptide was incubated with phosphorylated Akt (Ser-473) antibody at 4 °C for 2 hours before incubating with the tissue section. **Scale bar** = 25 μm.

protein kinases examined. The three-dimensional space in the ATP-binding pocket of PI3K is larger than the corresponding spaces found in the ATP-binding pockets of other protein kinases *(44)*. The triazine and morpholino groups of ZSTK474 fit well into this space. Therefore, these moieties may be important in the specificity of ZSTK474 for PI3K. To further confirm the binding of ZSTK474 to the ATP-binding pocket of PI3K, a biochemical experiment that examines whether ZSTK474 competitively inhibits the binding of ATP to its binding site is required.

PI3K plays an important role in the proliferation of tumor cells. We compared ZSTK474 with other PI3K inhibitors, LY294002 and wortmannin, for its ability to inhibit cell proliferation. At concentrations of less than 1 μM, ZSTK474 potently inhibited the growth of various cancer cell lines. The growth inhibitory activity of ZSTK474 was more than 10-fold stronger than that of wortmannin, which may be due to wortmannin's being somewhat unstable in cell culture medium *(48)*, or of LY294002, which may be due to the PI3K inhibitory activity of LY294002 being more than 10-fold weaker than that of ZSTK474. Furthermore, the PI3K inhibitory activities of other *s*-triazine derivatives statistically significantly correlated with their cell growth inhibitory activities. These results suggested that ZSTK474 inhibited cell

growth by inhibiting PI3K, with subsequent inhibitory effects on downstream signaling molecules.

PI3K participates in the induction of the membrane ruffling. ZSTK474 inhibited platelet-derived growth factor–induced membrane ruffling in murine embryonic fibroblast cells, which is an Akt-independent process, and inhibited the generation of PIP_3. These results demonstrate that ZSTK474 inhibited PI3K activity in intact cells.

Because the PI3K pathway is considered to mediate antiapoptotic signals in tumor cells, ZSTK474 was expected to induce apoptosis efficiently by inhibiting PI3K. However, we observed weak or no induction of apoptosis after ZSTK474 treatment in OVCAR3 cells or A549 cells, respectively. Therefore, induction of apoptosis by ZSTK474 appears to be a cell type–dependent event, probably because of the differential status of the PI3K signaling pathway in various cancer cell lines.

One of the major downstream effectors of PI3K is Akt, a serine/threonine protein kinase. Therefore, we investigated the effect of PI3K on the activation of Akt and its key downstream components. ZSTK474 reduced, in a time-dependent manner, phosphorylation of the protein kinases Akt and GSK-3β and the expression of cyclin D1 protein. Akt inhibits cyclin D1 degradation by regulating the activity of GSK-3β *(49)*. After its phosphorylation by GSK-3β, cyclin D1 is targeted for degradation by the proteasome. Akt phosphorylates GSK-3β directly and blocks its kinase activity, thereby allowing cyclin D1 to accumulate in cells *(49)*. ZSTK474 inhibited the phosphorylation of other downstream signaling components that are involved in regulating cell proliferation (i.e., FKHRL1, FKHR, TSC-2, mTOR, and p70S6K) in a dose-dependent manner. These results indicated that the inhibition of PI3K by ZSTK474 was followed by a decrease in relevant downstream signaling, which may in turn facilitate cell growth inhibition. In fact, we observed complete G_1-phase arrest in A549 cells after ZSTK474 treatment. In contrast, ZSTK474 did not inhibit phosphorylation of either ERK1/2 or MEK1/2, suggesting that ZSTK474 does not inhibit components in the RAS–ERK pathway.

Orally administered ZSTK474 displayed potent antitumor activity against human cancer xenografts in mice, without evidence of critical toxicity. Known PI3K inhibitors—such as LY294002 *(46,50–52)*, wortmannin *(53,54)*, and viridin analogues *(54)*—have previously been examined for their antitumor activities. In most reports, LY294002, which was administered intraperitoneally because it is insoluble in water, had antitumor activity when administered at an early stage (i.e., within 7 days after inoculation of tumor cells) *(50)*, but it also induced severe dermal toxicity *(46)*. Wortmannin also had antitumor activity, but again it achieved sufficient efficacy only when administered at an early stage *(53)*, and it caused liver toxicity *(54)*. An analogue of wortmannin, PX-866, has recently been developed *(54)* that has better efficacy and lower toxicity than wortmannin. However, this agent still produces liver toxicity *(54)*. In this study, we found that ZSTK474 had strong antitumor efficacy against advanced-stage tumors (i.e., >15 days after inoculation of tumor cells) and that ZSTK474 did not produce noticeable toxicity in critical organs after daily administration for more than 14 days. We also confirmed reduction of Akt phosphorylation after ZSTK474 administration. Thus, the reduction of Akt phosphorylation may be a useful biomarker marker to monitor the efficacy of ZSTK474 in future investigations of ZSTK474.

Although ZSTK474 indicated favorable features for a novel anticancer drug candidate as described above, various preclinical studies remain before ZSTK474 can be evaluated in a clinical trial, which include more precise investigation of the molecular pharmacology, analyses of the pharmacokinetics and the pharmacodynamics, and careful investigation of the toxicity. Investigation of the toxicity derived from PI3K inhibition is especially important because PI3K is expressed in various normal tissues. These studies are currently under way.

In conclusion, we demonstrated that the compound ZSTK474 is a new PI3K inhibitor and that it has strong antitumor activity against human cancer xenografts without critical toxicity. It appears that ZSTK474 can be orally administered over long periods, which may be important for the treatment of cancer. Thus, ZSTK474 merits further investigation as an anticancer drug.

References

(1) Auger KR, Serunian LA, Soltoff SP, Libby P, Cantley LC. PDGF-dependent tyrosine phosphorylation stimulates production of novel polyphosphoinositides in intact cells. Cell 1989;57:167–75.

(2) Whitman M, Downes CP, Keeler M, Keller T, Cantley L. Type I phosphatidylinositol kinase makes a novel inositol phospholipid, phosphatidylinositol-3-phosphate. Nature 1988;332:644–6.

(3) Vivanco I, Sawyers CL. The phosphatidylinositol 3-Kinase AKT pathway in human cancer. Nat Rev Cancer 2002;2:489–501.

(4) Luo J, Manning BD, Cantley LC. Targeting the PI3K-Akt pathway in human cancer: rationale and promise. Cancer Cell 2003;4:257–62.

(5) Aoki M, Schetter C, Himly M, Batista O, Chang HW, Vogt PK. The catalytic subunit of phosphoinositide 3-kinase: requirements for oncogenicity. J Biol Chem 2000;275:6267–75.

(6) Jimenez C, Jones DR, Rodriguez-Viciana P, Gonzalez-Garcia A, Leonardo E, Wennstrom S, et al. Identification and characterization of a new oncogene derived from the regulatory subunit of phosphoinositide 3-kinase. EMBO J 1998;17:743–53.

(7) Samuels Y, Wang Z, Bardelli A, Silliman N, Ptak J, Szabo S, et al. High frequency of mutations of the PIK3CA gene in human cancers. Science 2004;304:554.

(8) Levine DA, Bogomolniy F, Yee CJ, Lash A, Barakat RR, Borgen PI, et al. Frequent mutation of the PIK3CA gene in ovarian and breast cancers. Clin Cancer Res 2005;11:2875–8.

(9) Shayesteh L, Lu Y, Kuo WL, Baldocchi R, Godfrey T, Collins C, et al. PIK-3CA is implicated as an oncogene in ovarian cancer. Nat Genet 1999;21: 99–102.

(10) Pedrero JM, Carracedo DG, Pinto CM, Zapatero AH, Rodrigo JP, Nieto CS, et al. Frequent genetic and biochemical alterations of the PI 3-K/AKT/PTEN pathway in head and neck squamous cell carcinoma. Int J Cancer 2005;114:242–8.

(11) Kobayashi M, Nagata S, Iwasaki T, Yanagihara K, Saitoh I, Karouji Y, et al. Dedifferentiation of adenocarcinomas by activation of phosphatidylinositol 3-kinase. Proc Natl Acad Sci U S A 1999;96:4874–9.

(12) Steck PA, Pershouse MA, Jasser SA, Yung WK, Lin H, Ligon AH, et al. Identification of a candidate tumour suppressor gene, MMAC1, at chromosome 10q23.3 that is mutated in multiple advanced cancers. Nat Genet 1997;15:356–62.

(13) Lee HY, Srinivas H, Xia D, Lu Y, Superty R, LaPushin R, et al. Evidence that phosphatidylinositol 3-kinase- and mitogen-activated protein kinase kinase-4/c-Jun NH2-terminal kinase-dependent Pathways cooperate to maintain lung cancer cell survival. J Biol Chem 2003;278:23630–8.

(14) Czauderna F, Fechtner M, Aygun H, Arnold W, Klippel A, Giese K, et al. Functional studies of the PI*(3)*-kinase signalling pathway employing synthetic and expressed siRNA. Nucleic Acids Res 2003;31:670–82.

(15) Okada T, Sakuma L, Fukui Y, Hazeki O, Ui M. Blockage of chemotactic peptide-induced stimulation of neutrophils by wortmannin as a result of selective inhibition of phosphatidylinositol 3-kinase. J Biol Chem 1994;269:3563–7.

(16) Powis G, Bonjouklian R, Berggren MM, Gallegos A, Abraham R, Ashendel C, et al. Wortmannin, a potent and selective inhibitor of phosphatidylinositol-3-kinase. Cancer Res 1994;54:2419–23.

(17) Wipf P, Minion DJ, Halter RJ, Berggren MI, Ho CB, Chiang GG, et al. Synthesis and biological evaluation of synthetic viridins derived from C(20)-heteroalkylation of the steroidal PI-3-kinase inhibitor wortmannin. Org Biomol Chem 2004;2:1911–20.
(18) Woscholski R, Kodaki T, McKinnon M, Waterfield MD, Parker PJ. A comparison of demethoxyviridin and wortmannin as inhibitors of phosphatidylinositol 3-kinase. FEBS Lett 1994;342:109–14.
(19) Vlahos CJ, Matter WF, Hui KY, Brown RF. A specific inhibitor of phosphatidylinositol 3-kinase, 2-(4-morpholinyl)-8-phenyl-4H-1-benzopyran-4-one (LY294002). J Biol Chem 1994;269:5241–8.
(20) West KA, Castillo SS, Dennis PA. Activation of the PI3K/Akt pathway and chemotherapeutic resistance. Drug Resist Updat 2002;5:234–48.
(21) Workman P. Inhibiting the phosphoinositide 3-kinase pathway for cancer treatment. Biochem Soc Trans 2004;32:393–6.
(22) Yaguchi S, Izumisawa Y, Sato M, Nakagane T, Koshimizu I, Sakita K, et al. In vitro cytotoxicity of imidazolyl-1,3,5-triazine derivatives. Biol Pharm Bull 1997;20:698–700.
(23) Matsuno T, Karo M, Sasahara H, Watanabe T, Inaba M, Takahashi M, et al. Synthesis and antitumor activity of benzimidazolyl-1,3,5-triazine and benzimidazolylpyrimidine derivatives. Chem Pharm Bull (Tokyo) 2000;48:1778–81.
(24) Dan S, Tsunoda T, Kitahara O, Yanagawa R, Zembutsu H, Katagiri T, et al. An integrated database of chemosensitivity to 55 anticancer drugs and gene expression profiles of 39 human cancer cell lines. Cancer Res 2002;62: 1139–47.
(25) Yamori T. Panel of human cancer cell lines provides valuable database for drug discovery and bioinformatics. Cancer Chemother Pharmacol 2003; 52 Suppl 1:S74–9.
(26) Yamori T, Matsunaga A, Sato S, Yamazaki K, Komi A, Ishizu K, et al. Potent antitumor activity of MS-247, a novel DNA minor groove binder, evaluated by an in vitro and in vivo human cancer cell line panel. Cancer Res 1999;59:4042–9.
(27) Monks A, Scudiero D, Skehan P, Shoemaker R, Paull K, Vistica D, et al. Feasibility of a high-flux anticancer drug screen using a diverse panel of cultured human tumor cell lines. J Natl Cancer Inst 1991;83:757–66.
(28) Paull KD, Shoemaker RH, Hodes L, Monks A, Scudiero DA, Rubinstein L, et al. Display and analysis of patterns of differential activity of drugs against human tumor cell lines: development of mean graph and COMPARE algorithm. J Natl Cancer Inst 1989;81:1088–92.
(29) Fidler IJ. Biological behavior of malignant melanoma cells correlated to their survival in vivo. Cancer Res 1975;35:218–24.
(30) Skehan P, Storeng R, Scudiero D, Monks A, McMahon J, Vistica D, et al. New colorimetric cytotoxicity assay for anticancer-drug screening. J Natl Cancer Inst 1990;82:1107–12.
(31) Boyd MR. Status of the National Cancer Institute preclinical antitumor drug discovery screen: implications for selection of new agents for clinical trial. Vol 3. Philadelphia (PA): Lippincott; 1989.
(32) Fukui Y, Kornbluth S, Jong SM, Wang LH, Hanafusa H. Phosphatidylinositol kinase type I activity associates with various oncogene products. Oncogene Res 1989;4:283–92.
(33) Gray A, Olsson H, Batty IH, Priganica L, Peter Downes C. Nonradioactive methods for the assay of phosphoinositide 3-kinases and phosphoinositide phosphatases and selective detection of signaling lipids in cell and tissue extracts. Anal Biochem 2003;313:234–45.
(34) Rarey M, Kramer B, Lengauer T, Klebe G. A fast flexible docking method using an incremental construction algorithm. J Mol Biol 1996;261:470–89.
(35) Tsujishita H, Hirono S. CAMDAS: an automated conformational analysis system using molecular dynamics. Conformational Analyzer with Molecular Dynamics And Sampling. J Comput Aided Mol Des 1997;11:305–15.
(36) Radwan AA, Gouda H, Yamaotsu N, Torigoe H, Hirono S. Rational procedure for 3D-QSAR analysis using TRNOE experiments and computational methods: application to thermolysin inhibitors. Drug Des Discov 2001;17:265–81.
(37) Kuntz ID, Blaney JM, Oatley SJ, Langridge R, Ferrin TE. A geometric approach to macromolecule-ligand interactions. J Mol Biol 1982;161:269–88.
(38) Jones G, Willett P, Glen RC, Leach AR, Taylor R. Development and validation of a genetic algorithm for flexible docking. J Mol Biol 1997;267: 727–48.
(39) Eldridge MD, Murray CW, Auton TR, Paolini GV, Mee RP. Empirical scoring functions: I. The development of a fast empirical scoring function to estimate the binding affinity of ligands in receptor complexes. J Comput Aided Mol Des 1997;11:425–45.
(40) Muegge I, Martin YC. A general and fast scoring function for protein-ligand interactions: a simplified potential approach. J Med Chem 1999;42:791–804.
(41) Katsuki M, Chuang VT, Nishi K, Kawahara K, Nakayama H, Yamaotsu N, et al. Use of photoaffinity labeling and site-directed mutagenesis for identification of the key residue responsible for extraordinarily high affinity binding of UCN-01 in human alpha1-acid glycoprotein. J Biol Chem 2005;280:1384–91.
(42) Kimura K, Hattori S, Kabuyama Y, Shizawa Y, Takayanagi J, Nakamura S, et al. Neurite outgrowth of PC12 cells is suppressed by wortmannin, a specific inhibitor of phosphatidylinositol 3-kinase. J Biol Chem 1994;269:18961–7.
(43) Plank J, Rychlo A. [A method for quick decalcification.]. Zentralbl Allg Pathol 1952;89:252–4.
(44) Walker EH, Pacold ME, Perisic O, Stephens L, Hawkins PT, Wymann MP, et al. Structural determinants of phosphoinositide 3-kinase inhibition by wortmannin, LY294002, quercetin, myricetin, and staurosporine. Mol Cell 2000;6:909–19.
(45) Lawrie AM, Noble ME, Tunnah P, Brown NR, Johnson LN, Endicott JA. Protein kinase inhibition by staurosporine revealed in details of the molecular interaction with CDK2. Nat Struct Biol 1997;4:796–801.
(46) Hu L, Zaloudek C, Mills GB, Gray J, Jaffe RB. In vivo and in vitro ovarian carcinoma growth inhibition by a phosphatidylinositol 3-kinase inhibitor (LY294002). Clin Cancer Res 2000;6:880–6.
(47) Naasani I, Seimiya H, Yamori T, Tsuruo T. FJ5002: a potent telomerase inhibitor identified by exploiting the disease-oriented screening program with COMPARE analysis. Cancer Res 1999;59:4004–11.
(48) Holleran JL, Egorin MJ, Zuhowski EG, Parise RA, Musser SM, Pan SS. Use of high-performance liquid chromatography to characterize the rapid decomposition of wortmannin in tissue culture media. Anal Biochem 2003;323:19–25.
(49) Diehl JA, Cheng M, Roussel MF, Sherr CJ. Glycogen synthase kinase-3beta regulates cyclin D1 proteolysis and subcellular localization. Genes Dev 1998;12:3499–511.
(50) Su JD, Mayo LD, Donner DB, Durden DL. PTEN and phosphatidylinositol 3′-kinase inhibitors up-regulate p53 and block tumor-induced angiogenesis: evidence for an effect on the tumor and endothelial compartment. Cancer Res 2003;63:3585–92.
(51) Semba S, Itoh N, Ito M, Harada M, Yamakawa M. The in vitro and in vivo effects of 2-(4-morpholinyl)-8-phenyl-chromone (LY294002), a specific inhibitor of phosphatidylinositol 3′-kinase, in human colon cancer cells. Clin Cancer Res 2002;8:1957–63.
(52) Bondar VM, Sweeney-Gotsch B, Andreeff M, Mills GB, McConkey DJ. Inhibition of the phosphatidylinositol 3′-kinase-AKT pathway induces apoptosis in pancreatic carcinoma cells in vitro and in vivo. Mol Cancer Ther 2002;1:989–97.
(53) Lemke LE, Paine-Murrieta GD, Taylor CW, Powis G. Wortmannin inhibits the growth of mammary tumors despite the existence of a novel wortmannin-insensitive phosphatidylinositol-3-kinase. Cancer Chemother Pharmacol 1999;44:491–7.
(54) Ihle NT, Williams R, Chow S, Chew W, Berggren MI, Paine-Murrieta G, et al. Molecular pharmacology and antitumor activity of PX-866, a novel inhibitor of phosphoinositide-3-kinase signaling. Mol Cancer Ther 2004;3:763–72.

NOTES

We thank Dr. R. H. Shoemaker and Dr. K. D. Paull for discussion on the establishment of JFCR39 and COMPARE analysis; Ms. Y. Nishimura, Ms. M. Seki, Ms. Y. Mukai, Ms. M. Okamura, and Dr. Y. Yoshida for technical assistance; Mr. T. Watanabe, Dr. Y. Tsuchida and Mr. K. Saito for synthesis of compounds; and Mr. M. Takehara and Dr. M. Takahashi for advice on the study.

Supported by grants-in-aid of the Priority Area "Cancer" from the Ministry of Education, Culture, Sports, Science, and Technology, Japan, to T. Yamori (11177101); grants-in-aid for Scientific Research (B) from Japan Society for the Promotion of Science to T. Yamori (17390032); and a grant from National Institute of Biomedical Innovation, Japan, to T. Yamori (05-13).

Funding to pay the Open Access publication charges for this article was provided by the Japanese Foundation for Cancer Research.

Manuscript received September 16, 2005; revised January 23, 2006; accepted March 3, 2006.

THE JOURNAL OF BIOLOGICAL CHEMISTRY VOL. 281, NO. 25, pp. 17492–17500, June 23, 2006

Autotaxin Is Overexpressed in Glioblastoma Multiforme and Contributes to Cell Motility of Glioblastoma by Converting Lysophosphatidylcholine TO Lysophosphatidic Acid*

Received for publication, February 24, 2006 Published, JBC Papers in Press, April 19, 2006, DOI 10.1074/jbc.M601803200

Yasuhiro Kishi[‡], Shinichi Okudaira[‡], Masayuki Tanaka[‡], Kotaro Hama[‡], Dai Shida[§], Joji Kitayama[§], Takao Yamori[¶], Junken Aoki[‡1], Takamitsu Fujimaki[‖], and Hiroyuki Arai[‡]

From the [‡]Graduate School of Pharmaceutical Sciences, the University of Tokyo, 7-3-1 Hongo, Bunkyo-ku, Tokyo 113-0033, the [§]Graduate School of Medicine, the University of Tokyo, 7-3-1 Hongo, Bunkyo-ku, Tokyo 113-0033, the [¶]Division of Molecular Pharmacology, Cancer Chemotherapy Center, Japanese Foundation for Cancer Research, Toshima-ku, Tokyo 170-8455, and the [‖]Department of Neurosurgery, Teikyo University School of Medicine, 2-11-1, Kaga, Itabashi-ku, Tokyo 173-8605, Japan

Autotaxin (ATX) is a multifunctional phosphodiesterase originally isolated from melanoma cells as a potent cell motility-stimulating factor. ATX is identical to lysophospholipase D, which produces a bioactive phospholipid, lysophosphatidic acid (LPA), from lysophosphatidylcholine (LPC). Although enhanced expression of ATX in various tumor tissues has been repeatedly demonstrated, and thus, ATX is implicated in progression of tumor, the precise role of ATX expressed by tumor cells was unclear. In this study, we found that ATX is highly expressed in glioblastoma multiforme (GBM), the most malignant glioma due to its high infiltration into the normal brain parenchyma, but not in tissues from other brain tumors. In addition, LPA_1, an LPA receptor responsible for LPA-driven cell motility, is predominantly expressed in GBM. One of the glioblastomas that showed the highest ATX expression (SNB-78), as well as ATX-stable transfectants, showed LPA_1-dependent cell migration in response to LPA in both Boyden chamber and wound healing assays. Interestingly these ATX-expressing cells also showed chemotactic response to LPC. In addition, knockdown of the ATX level using small interfering RNA technique in SNB-78 cells suppressed their migratory response to LPC. These results suggest that the autocrine production of LPA by cancer cell-derived ATX and exogenously supplied LPC contribute to the invasiveness of cancer cells and that LPA_1, ATX, and LPC-producing enzymes are potential targets for cancer therapy, including GBM.

Autotaxin (ATX)[2] is a 125-kDa glycoprotein and a potent tumor cell motogen that was originally isolated from the conditioned medium of A2058 human melanoma cells as a cell motility-stimulating factor for melanoma cells (1). ATX was subsequently identified as a member of a family of ecto/exoenzymes referred to as nucleotide pyrophosphatases/phosphodiesterases (NPPs) (2, 3). The three cloned members of this family (PC-1/NPP1, ATX/NPP2, and B-10/NPP3) share a 47–55% amino acid sequence identity. PC-1/NPP1 and B-10/NPP3 hydrolyze 5′-phosphodiester bonds in nucleotides *in vitro*, whereas ATX/NPP2 shows only weak activity at hydrolyzing such bonds. ATX is synthesized as a type II membrane protein and is released from cells in a soluble form by an unknown mechanism (3, 4). Enhanced expression of ATX in Ras-transformed NIH3T3 cells greatly enhances their invasive, tumorigenic, and metastatic potentials (5). In addition, enhanced expression of ATX has been repeatedly demonstrated in various malignant tumor tissues including non-small cell lung cancer (6), breast cancer (7, 8), renal cell cancer (9), hepatocellular carcinoma (10, 11), and thyroid cancer (12), suggesting that ATX confers the tumorigenic and metastatic potentials of cancer cells. However, there is no direct evidence to show such a hypothesis so far.

The mechanism by which ATX exhibits its biological activity toward various cancer cells was unknown. An ATX point mutant that is deficient in 5′-nucleotide phosphodiesterase activity was found to abolish the cell motility-stimulating activity of ATX (13), indicating that the migratory response to ATX requires an intact catalytic site. Recently, we and others showed that ATX has lysophospholipase D (lysoPLD) activity, which catalyzes a reaction to produce a bioactive lysophospholipid, lysophosphatidic acid (LPA), from lysophosphatidylcholine (LPC) (14, 15). ATX has a significantly lower K_m for LPC than the K_m for the classical nucleotide substrate. Because LPA has long been defined as a cell motility-stimulating factor for various cell types including glioblastomas (16–18), ATX has been suggested to regulate motility by producing LPA through the G-protein-coupled receptor. Indeed, recent studies have shown that ATX stimulates the cell motility of various cancer cells *in vitro* through one of the LPA receptors, LPA_1 (19–22). Taking account of the fact that elevated ATX expression has been detected in various tumors (6–12), it is possible that certain cancer cells utilize the ATX-LPC-LPA-LPA_1 system for their motility. In these cells, a possible regulatory factor that remains to be characterized is LPC. LPC is always present in plasma. In human plasma, its concentration ranges from 100 to 300 μM. LPC is also detected in other biological fluids such as seminal fluids and cerebrospinal fluids and in tissues and various types of cells but at much lower concentrations than in plasma (23, 24).

Glioblastoma multiforme (GBM) is a highly malignant brain tumor. Removal of the tumor mass transiently improves the condition of the patient, but the ability of GBM cells to infiltrate normal brain tissue invariably almost always leads to tumor recurrence. Thus, most patients experience recurrence within 1 year (25), and less than 20% of the patients survive more than 2 years (26). GBM cells (glioblastomas) are highly motile and invade the normal brain parenchyma diffusely (27). Several factors responsible for their invasive phenotype have been

* The costs of publication of this article were defrayed in part by the payment of page charges. This article must therefore be hereby marked "*advertisement*" in accordance with 18 U.S.C. Section 1734 solely to indicate this fact.

[1] To whom correspondence should be addressed. Tel.: 81-3-5841-4723; Fax: 81-3-3818-3173; E-mail: jaoki@mol.f.u-tokyo.ac.jp.

[2] The abbreviations used are: ATX, autotaxin; GBM, glioblastoma multiforme; LPA, lysophosphatidic acid; LPC, lysophosphatidylcholine; lysoPLD, lysophospholipase D; RT, reverse transcription; BBB, blood-brain barrier; NPP, nucleotide pyrophosphatases/phosphodiesterases; CNS, central nervous system; siRNA, small interfering RNA; GAPDH, glyceraldehyde-3-phosphate dehydrogenase.

reported, such as certain extracellular matrix proteins including laminin, fibronectin, and/or collagen can promote glioma cell migration (28, 29). Secreted matrix metalloproteinases remodel the extracellular matrix, creating pathways more conducive to migration through normal brain tissue (30). Investigations of the factors that affect the motility of glioblastomas are of particular interest because an understanding of these factors is needed for valid GBM therapy. Because the blood-brain barrier (BBB) is disrupted in GBM tissue, some components in plasma might affect the cell motility of glioblastomas (31, 32). In this study, we examined the expression of ATX and LPA_1 in brain tumor tissues and various tumor cell lines and found that both ATX and LPA_1 are predominantly expressed in glioblastomas and GBM tissue. Using glioblastomas as a model system, we evaluated the effects of ATX, LPA_1, LPA, and LPC on the motility of the cells.

MATERIALS AND METHODS

Reagents—1-oleoyl-LPA (18:1) and 1-oleoyl-LPC (18:1) was purchased from Avanti Polar Lipids Inc. (Alabaster, AL). Ki16425 was kindly provided by Dr. Hideo Ohata (Kirin Brewery Co., Takasaki, Japan).

Cell Lines—All human tumor cell lines were maintained in RPMI 1640 (Sigma) supplemented with 2 mM glutamine, 1× penicillin/streptomycin, and 5% (v/v) heat-inactivated fetal bovine serum as described previously (33). The cell lines used in this study were NCI-H23 (lung), NCI-H226 (lung), NCI-H522 (lung), NCI-H460 (lung), A549 (lung), DMS273 (lung), DMS114 (lung), HCC-2998 (colon), HT-29 (colon), WiDr (colon), HCT-15 (colon), DLD1 (colon), SW480 (colon), LOVO (colon), CaRI (rectum), WiDr (colon), CaCo2 (colon), Colo320 (colon), Colo201 (colon), HCT-116 (colon), KM12 (colon), HT1080 (colon), RXF-631L (renal), ACHN (renal), OVCAR3 (ovary), OVCAR4 (ovary), OVCAR5 (ovary), OVCAR8 (ovary), SKOV-3 (ovary), U251 (CNS), SF295 (CNS), SF539 (CNS), SF268 (CNS), SNB75 (CNS), SNB78 (CNS), MKN45 (stomach), MKN28 (stomach), St4 (stomach), MKN1 (stomach), MKN7 (Stomach), MKN74 (stomach), KatoIII (stomach), MKN28 (stomach), MKN45 (stomach), MKN74 (stomach), MDA-MB231 (breast), HBC4(breast), BSY1 (breast), MCF7 (breast), DU145 (prostate), PC3 (prostate), HPC5 (others), A2058 (melanoma), and HeLa (uterine cervix). Mouse 203G glioma cells were maintained in RPMI 1640 supplemented with 2 mM glutamine, 1× penicillin/streptomycin, and 10% (v/v) heat-inactivated fetal bovine serum. This cell line was kindly provided by Dr. Koji Adachi (Nippon Medical School Tokyo, Japan).

Quantitative Real-time RT-PCR—From various cancer tissues and cancer cell lines, total RNA from cells was isolated using ISOGEN (Nippongene, Toyama, Japan) and reverse-transcribed using the SuperScript first-strand synthesis system for RT-PCR (Invitrogen). Oligonucleotide primers for PCR were designed using Primer Express Software (Applied Biosystems, Foster City, CA). The sequences of the oligonucleotides used in PCR were as follows: ATX (human), forward, 5′-GGGTGAAAGCTGGAACATTCTT-3′; ATX (human), reverse, 5′-GCCACCGCAATATGGAATTATAAG-3′; LPA_1 (human), forward, 5′-AATCGGGATACCATGATGAGTCTT-3′; LPA_1 (human), reverse, 5′-CCAGGAGTCCAGCAGATGATAAA-3′; LPA_2 (human), forward, 5′-CGCTCAGCCTGGTCAAGACT-3′; LPA_2 (human), reverse, 5′-TTGCAGGACTCACAGCCTAAAC-3′; LPA_3 (human), forward, 5′-AGGACACCCATGAAGCTAATGAA-3′; LPA_3 (human), reverse, 5′-GCCGTCGAGGAGCAGAAC-3′; LPA_4 (human), forward, 5′-CCTAGTCCTCAGTGGCGGTATT-3′; LPA_4 (human), reverse, 5′-CCTTCAAAGCAGGTGGTGGTT-3′; ATX (mouse), forward, 5′-GGAGAATCACACTGGGTAGATGATG-3′; ATX (mouse), reverse, 5′-ACGGAGGGCGGACAAAC-3′; LPA_1 (mouse), forward, 5′-GAGGAATCGGGACACCATGAT-3′; LPA_1 (mouse), reverse, 5′-ACATCCAGCAATAACAAGACCAATC-3′; LPA_2 (mouse), forward, 5′-GACCACACTCAGCCTAGTCAAGAC-3′; LPA_2 (mouse), reverse, 5′-CTTACAGTCCAGGCCATCCA-3′; LPA_3 (mouse), forward, 5′-GCTCCCATGAAGCTAATGAAGACA-3′; LPA_3 (mouse), reverse, 5′-AGGCCGTCCAGCAGCAGA-3′; LPA_4 (mouse), forward, 5′-CAGTGCCTCCCTGTTTGTCTTC-3′; LPA_4 (mouse), reverse, 5′-GAGAGGGCCAGGTTGGTGAT-3′; GAPDH (human/mouse), forward, 5′-GCCAAGGTCATCCATGACAACT-3′; GAPDH (human/mouse), reverse, 5′-GAGGGGCCATCCACAGTCTT.

PCR reactions were performed using an ABI Prism 7000 sequence detection system (Applied Biosystems). The transcript number of human GAPDH was quantified, and each sample was normalized on the basis of GAPDH content.

LysoPLD Assay—Samples were incubated with 2 mM LPC (14:0) in the presence of 100 mM Tris-HCl (pH 9.0), 500 mM NaCl, 5 mM $MgCl_2$, and 0.05% Triton X-100 during indicated hours at 37 °C. The liberated choline was detected by an enzymatic photometric method as described (14). Briefly, the liberated choline was oxidized by choline oxidase, and the hydrogen peroxide generated was quantified using horseradish peroxidase and TOOS reagent (*N*-ethyl-*N*-(2-hydroxy-3-sulfoproryl)-3-methylanikine, Dojin, Tokyo, Japan).

SDS-PAGE/Western Blotting—Both cells and cell media were used to test for ATX protein expression. Cells were homogenized in phosphate-buffered saline, and then the cell homogenates were separated into membrane and soluble fractions by centrifugation at 100,000 × *g* for 60 min. Protein samples were separated by SDS-PAGE and transferred to nitrocellulose membranes using the Bio-Rad protein transfer system. The membranes were blocked with 10 mM Tris-HCl (pH 7.5) containing 150 mM sodium chloride, 5% (w/v) skimmed milk, and 0.05% (v/v) Tween 20, incubated with anti-lysoPLD monoclonal antibody (3D1) (23), and then treated with anti-rat IgG-horseradish peroxidase. Proteins bound to the antibody were visualized with an enhanced chemiluminescence kit (ECL, Amersham Biosciences).

Isolation of Stable ATX Transfectant—The plasmid vector pCAGGS (kindly provided by Dr. Junichi Miyazaki (34)) was utilized to create rat ATX (ATX-t) tagged with the Myc epitope at the C terminus (pCAGGS-rATX-Myc). To establish stable transfectants, 203G glioma cells were transfected with pCAGGS-rATX-Myc using Lipofectamine Plus reagents (Invitrogen) as recommended by the manufacturer and were grown in RPMI 1640 containing 800 μg/ml G418 (Wako). Individual G418-resistant clones were isolated by limiting dilution and screened by immunocytochemistry using Myc antibody and by measuring the lysoPLD activities of the culture media.

Recombinant ATX Preparations—Rat ATX was expressed and partially purified using baculovirus system as described previously (14). The purified ATX was dialyzed in phosphate-buffered saline and used for cell motility assays.

Boyden Chamber Assay—Chemotaxis was assayed as described previously (21). In brief, polycarbonate filters with 8-μm pores (Neuro-Probe, Inc., Gaithersburg, MD) were coated with 0.001% fibronectin (Sigma). Cells (1×10^5 cells in 200 μl/well) were loaded into the upper chambers and incubated at 37 °C for 6 h to allow migration. Cell migration to the bottom of the filter was evaluated by measuring optical density at 590 nm. For Ki16425 treatment, cells were preincubated with 1 μM Ki16425 for 30 min.

Wound Healing Assay—Cells were plated in cell culture plates (12-well) using cell growth media containing fetal bovine serum. After the cells had reached semiconfluence, fetal bovine serum was removed from the media and replaced with serum-free media. A plastic pipette tip was drawn across the center of the plate to produce a clean wound area 24 h

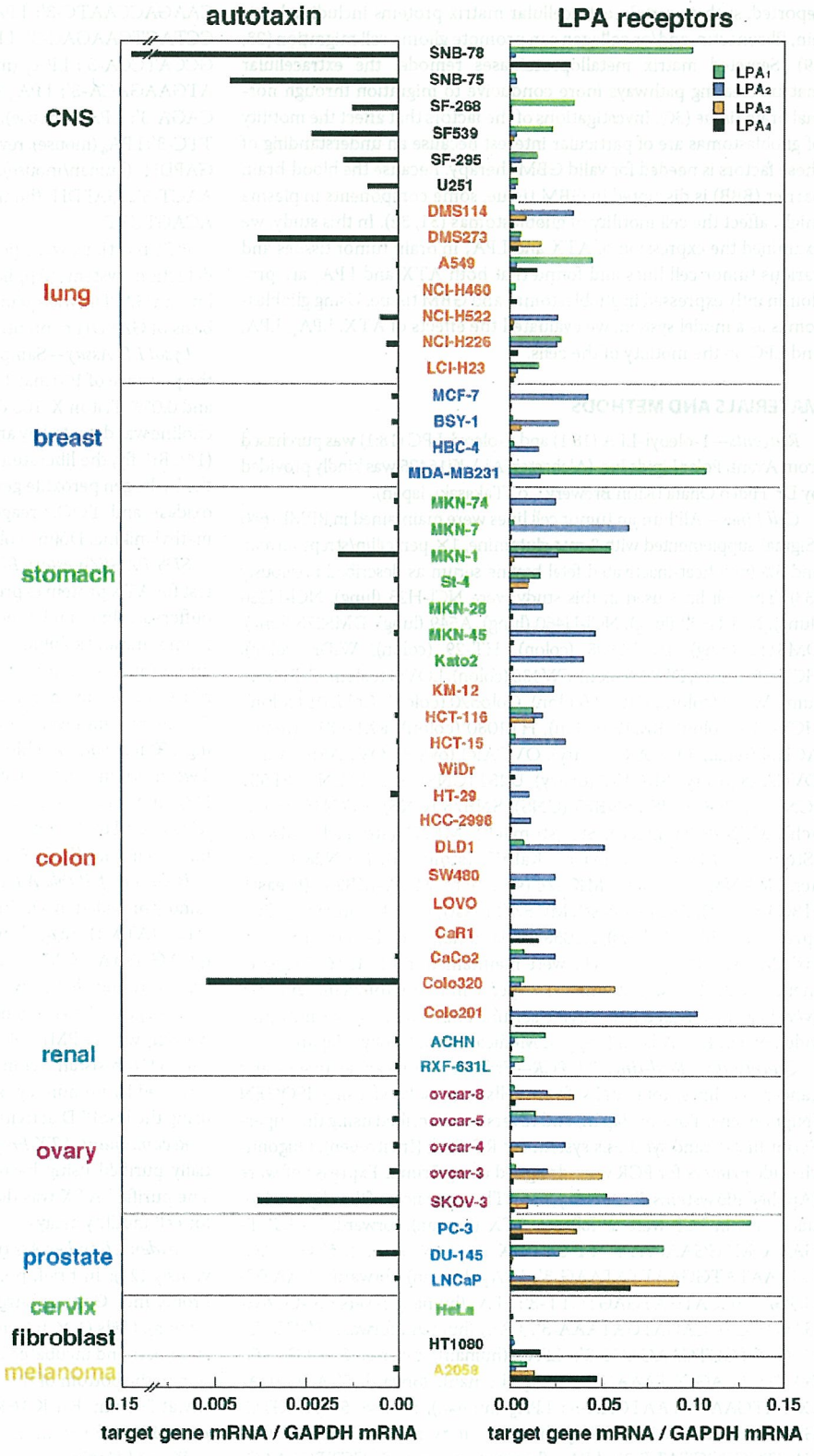

FIGURE 1. **Expression profiles of ATX and LPA receptors in tumor cell lines.** A quantitative RT-PCR analysis of ATX (*left*) and LPA receptors (LPA_1, LPA_2, LPA_3, and LPA_4, *right*) in 50 tumor cell lines from various origins (CNS, lung, breast, stomach, colon, kidney, ovary, prostate, cervix, fibroblast, and melanoma) was performed. Values are expressed relative to the expression of GAPDH mRNA.

after serum depletion. Medium was then replaced with serum-free medium containing different concentrations of 1-oleoyl-LPA, 1-oleoyl-LPC, Ki16425 (1 μM) and lysoPLD. After the cells were cultured for 12, 24, or 36 h, cell movement into the wound area was examined. The migration distances between the leading edge of the migrating cells and the edge of the wound were compared.

Quantification of LPC—LPC concentration in cell culture supernatant was determined as described previously (35). Briefly, cells were

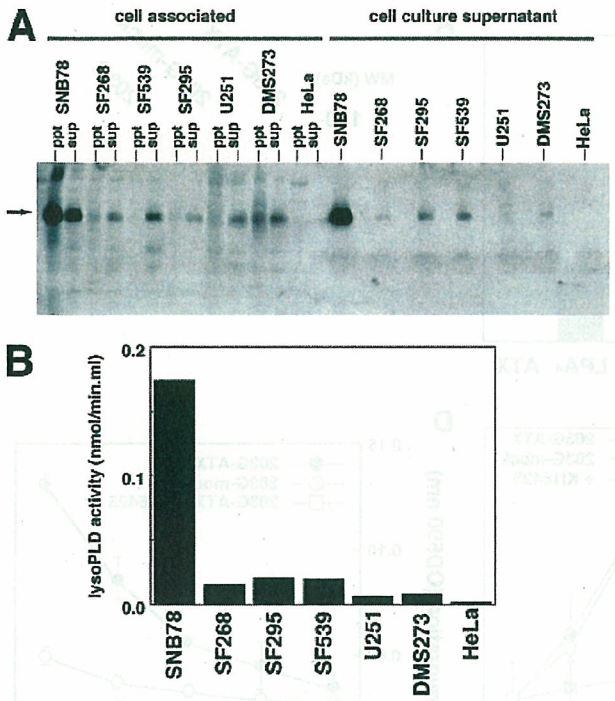

FIGURE 2. **ATX protein and lysoPLD activity in glioblastoma cell lines.** *A*, Western blot of cell membrane fractions (*ppt*), soluble fraction (*sup*), and cell culture medium using anti-human ATX monoclonal antibody 3D1. *B*, lysoPLD activity of culture media from glioblastoma and other cancer cell lines. LPC was used as the substrate.

cultured in serum-free RPMI 1640 containing 0.1% fatty acid-free bovine serum albumin (Sigma) for 2 days. LPC was extracted from culture media using the Bligh and Dyer method (51) and resuspended in phosphate-buffered saline containing 0.1% bovine serum albumin. LPC concentration was determined by a recently developed enzymatic colorimetric method as described. Briefly, samples were treated with lysophospholipase, glycerophosphorylcholine, phosphodiesterase, and choline oxidase. The resulting hydrogen peroxide generated was quantified using horseradish peroxidase and TOOS reagent.

RNA Interference—SNB-78 glioblastoma cells were transfected with siRNA oligonucleotide duplexes 1 day after confluence (day −1) with trans-it TKO (Takara, Kyoto, Japan) according to the manufacturer's instructions. Generally 20 nM siRNA was transfected with 0.5 μl of Lipofectamine per well of a 24-well plate with fresh media. Each experiment contained equivalent samples transfected with a non-targeting control siRNA pool and samples not treated with trans-it TKO. siRNA oligonucleotide duplexes for each gene of interest were purchased from WAKO (Osaka, Japan) as optimized single duplexes (ATX1, sense, 5′-gccguuggagucaauaucuGC-3′, antisense, 5′-agauauugacuccaacggcAA-3′ and ATX2, sense, 5′-gggagacugcuguaccaauTA-3′, antisense, 5′-auugguacagcagucucccCT-3′). Transfection efficiency was monitored using fluorescent (Cy3)-tagged oligonucleotides (Blockit, Invitrogen) transfected as described above and visualized with a mercury lamp fluorescent microscope.

RESULTS

Expression of ATX and LPA Receptors in 50 Tumor Cell Lines—We examined the expression of ATX in 50 cultured human tumor cell lines derived from various tumors using the quantitative RT-PCR technique. We found that some cells expressed a significant amount of ATX at both the mRNA and the protein levels (Figs. 1 and 2). High ATX expression was detected in DMS273 (lung cancer), colo320 (colon cancer), SKOV3

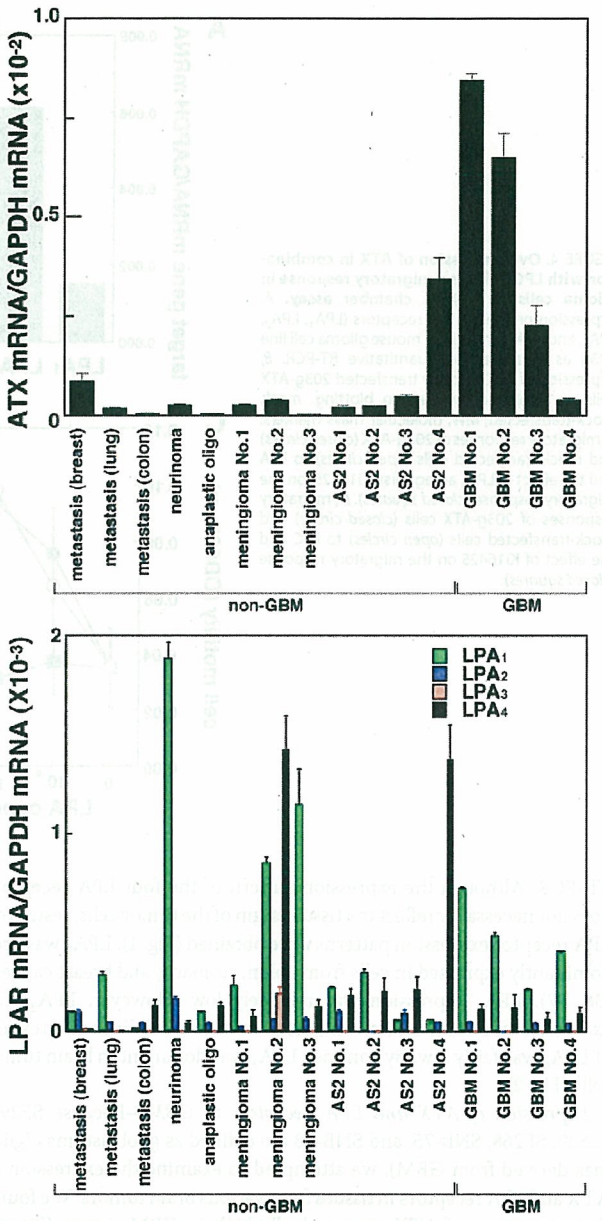

FIGURE 3. **Enhanced expression of ATX in GBM tissues.** Expressions of ATX (*A*) and LPA receptors (LPA_1, LPA_2, LPA_3, and LPA_4) (*B*) in various brain tumor tissues as measured by quantitative RT-PCR. Of the three LPA receptors (*LPAR*), LPA_1 has the highest expression in various brain tumors, possibly reflecting the high LPA_1 expression in normal human brain. Note that tissues AS2 number 4 and GBM number 1 are derived from the same patient. The patient's cancer was initially diagnosed as astrocytoma, and after the recurrence, it was diagnosed as GBM.

(ovarian cancer), MKN1 (stomach cancer), and most of the brain cancer cells (SF295, SF539, SF268, SNB-75, and SNB-78). The expression was highest in SNB-78 cells. In good agreement with this observation, both ATX protein and lysophospholipase D activity were detected in the culture supernatants of these ATX-positive cells (Fig. 2). Most of the protein was detected in the culture cell supernatants, whereas a small amount was detected in cells (Fig. 2*A*). These results confirm that ATX is secreted from cells, although ATX is initially biosynthesized in cells as a type II membrane protein.

We also examined the expression of the LPA receptors (LPA_1, LPA_2, LPA_3, and LPA_4) in the 50 human tumor cell lines using quantitative

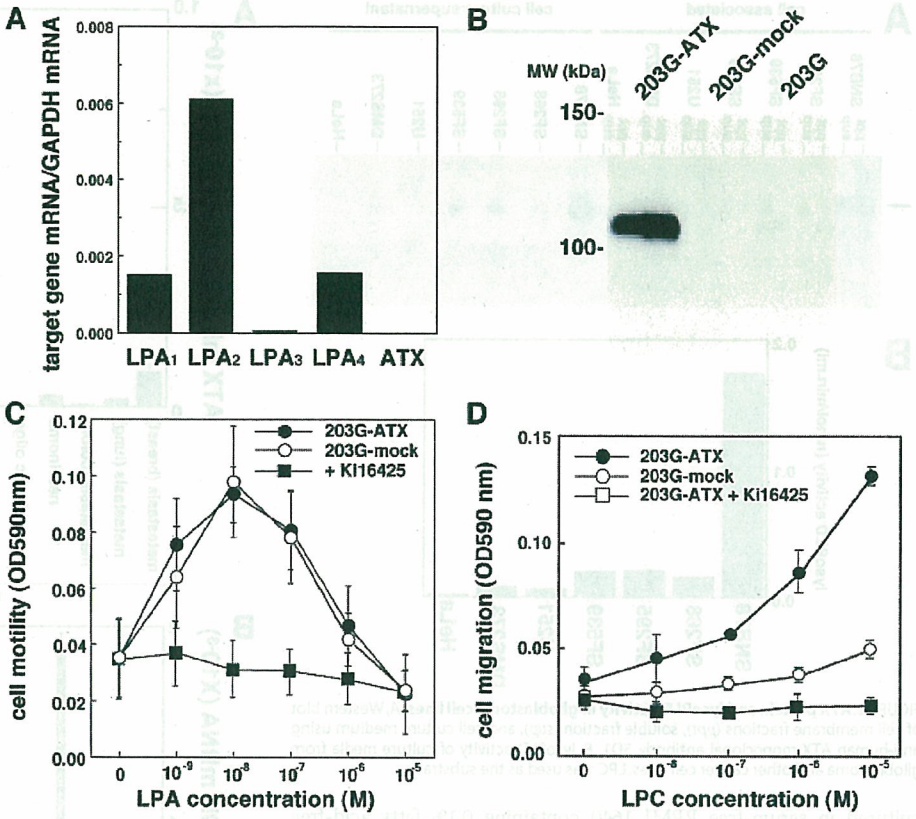

FIGURE 4. **Overexpression of ATX in combination with LPC induces a migratory response in glioma cells in Boyden chamber assay.** *A*, expression profiles of LPA receptors (LPA_1, LPA_2, LPA_3, and LPA_4) and ATX in mouse glioma cell line 203g as measured by quantitative RT-PCR. *B*, expression of ATX in stably transfected 203g-ATX cells as measured by Western blotting. *mock*, mock-transfected; *MW*, molecular mass markers. *C*, migratory responses of 203g-ATX (*closed circles*) and mock-transfected cells (*open circles*) to LPA and the effect of LPA_1 antagonist, Ki16425, on the migratory response (*closed squares*). *D*, migratory responses of 203g-ATX cells (*closed circles*) and mock-transfected cells (*open circles*) to LPC and the effect of Ki16425 on the migratory response (*closed squares*).

RT-PCR. Although the expression pattern of the four LPA receptors does not necessarily reflect the tissue origin of the tumor cells, restricted LPA receptor expression patterns were obtained (Fig. 1). LPA_2 was predominantly expressed in cells from colon, stomach, and breast cancers (36, 37). LPA_3 expression was relatively low. However, LPA_3 was expressed by certain ovarian and prostate cancer cell lines. Expression of LPA_4 was fairly low. By contrast, LPA_1 was dominant in brain tumor cells (Fig. 2).

Expression of ATX and LPA Receptors in GBM—Because SF295, SF539, SF268, SNB-75, and SNB-78 are defined as glioblastomas (gliomas derived from GBM), we attempted to examine the expression of ATX and LPA receptors in tissues from various brain tumors. We found that expression of ATX was markedly high in GBM tissues (Fig. 3). Three of four GBM tissue samples showed extremely high ATX expression. ATX expression is apparently lower in tissues from other brain tumors. One exception is a patient of astrocytoma (case AS2 number 4) whose tissue showed high ATX expression. He experienced early recurrence after only 16 months, and the tumor progressed to GBM at recurrence (case GBM number 1). Among the four LPA receptors, LPA_1 was dominantly expressed in most brain tumor tissues tested including GBM with low expression of LPA_2, LPA_3, and LPA_4, which may reflect the expression pattern in normal brain tissues (38, 39). The expression pattern of ATX and LPA receptors in GBM tissues indicates that ATX contributes to the invasive property of glioblastomas by producing LPA.

LPC Stimulates Cell Motility of ATX-expressing Cells—To test the possibility that glioblastomas acquire their high invasiveness through autocrine production of LPA by ATX, we first examined the effect of enhanced ATX expression on cell motility. We used mouse glioma cell line 203G that expressed LPA_1 (Fig. 4*A*) but not a detectable amount of ATX (Fig. 4*B*). 203G glioma cells that stably express ATX (203G-ATX) were established by transfecting ATX cDNA and by selecting neomycin-resistant clones. The established three lines expressed significant levels of ATX as judged by both lysoPLD activity (data not shown) and Western blotting (Fig. 4*B*). In addition, these cell lines showed similar expression pattern of LPA receptors to the parental 203G cells (data not shown). The effects of LPA on the motility of transfected cells and mock-transfected 203G cells in the Boyden chamber were similar (Fig. 4*C*). LPA had a similar effect on the motility of parental 203G cells (not shown). The effect of LPA on the motility of these cells was abolished by the LPA_1 antagonist, Ki16425 (Fig. 4*C*). By contrast, these cells showed quite distinct responses to LPC. LPC significantly stimulated the migration of 203G-ATX cells in Boyden chamber assay (Fig. 4*D*). However, a similar response was not induced in mock-transfected 203G cells (Fig. 4*D*) or in parental 203G cells (not shown). In addition, the stimulatory effect of LPC in 203G-ATX cells was completely abolished by the addition of Ki16425 (Fig. 4*D*), showing that LPA mediates the LPC-stimulated cell migration of the cells through LPA_1. We confirmed that platelet-derived growth factor induced similar migratory response in ATX-overexpressing, mock-transfected, and parental 203G cells (data not shown).

We further examined the role of endogenously expressed ATX in the cell motility of ATX-expressing cells, which has not been previously demonstrated so far. For this experiment, we used SNB-78, which has the highest ATX expression among the 50 tumor cell lines (Fig. 1). As shown in Fig. 5*A*, SNB-78 cells, like other LPA_1-positive cells, showed a migratory response to exogenous LPA in the Boyden chamber. LPC also stimulated the migration of SNB-78 (Fig. 5*B*). Ki16425 blocked not only the LPA-induced migratory response but also the LPC-induced migratory response (Fig. 5). This indicates that: 1) LPC is converted to LPA by the lysoPLD activity of endogenous ATX, 2) the LPA generated subse-

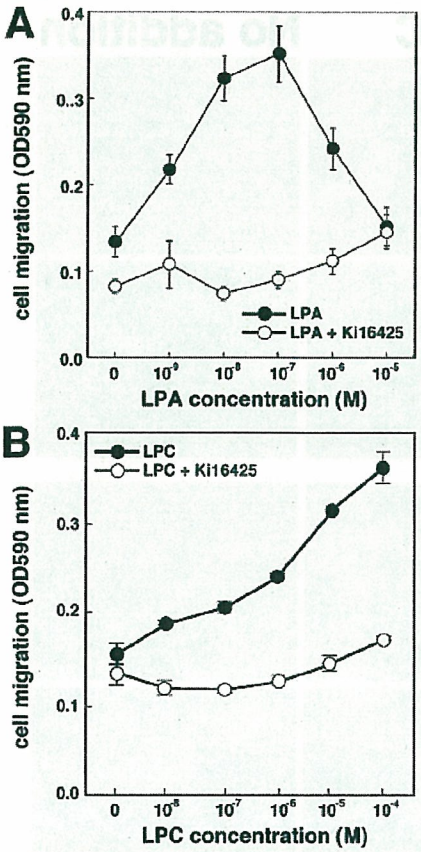

FIGURE 5. **Effects of LPA and LPC on migration of glioblastoma cells.** Migration of SNB-78 glioblastoma cells in response to LPA (*A*, *closed circles*) and LPC (*B*, *closed circles*) was measured with a Boyden chamber. Both responses were abolished by Ki16425 (*open circles*).

quently stimulates cell migration through LPA_1, and 3) LPC behaves as a chemotactic factor toward ATX-expressing cells.

We previously showed that LPC is released from cells and could be converted to LPA to induce cell migration by exogenously added ATX (14). In fact, SNB-78 was found to release a small amount of LPC into the cell culture medium, and the amount gradually increased during the culture (data not shown). However, we were unable to evaluate the effect of cell-derived LPC on cell motility in the Boyden chamber since LPC is lost during preparation of the cells for the Boyden chamber assay. Accordingly, to evaluate the effects of cell-derived LPC and ATX on cell migration, we used a wound healing assay, which takes a relatively long period. As expected, exogenously added LPA was able to induce migration of SNB-78 cells in the wound healing assay (Fig. 6*A*). The migratory response was abolished by Ki16425, which shows that LPA_1 is involved in this system, as was observed in Boyden chamber assay (Fig. 6*A*). In the absence of exogenous LPC, we observed a weak migratory response, which was also blocked by Ki16425 (Fig. 6*B*), showing that endogenous LPC and ATX, to a lesser extent, contribute to the migration of SNB-78 cells. By contrast, strong migratory responses were observed when LPC (10 μM) was added to the cells. The migratory response induced by LPC was again inhibited by Ki16425 (Fig. 6*C*). The amount of LPC released from SNB-78 was ~50 nM as judged by the enzymatic colorimetric method for determination of LPC. This indicates that the amount of endogenous LPC released from SNB-78 is insufficient to induce a full migratory response in the cells and that exogenous LPC is potentially a

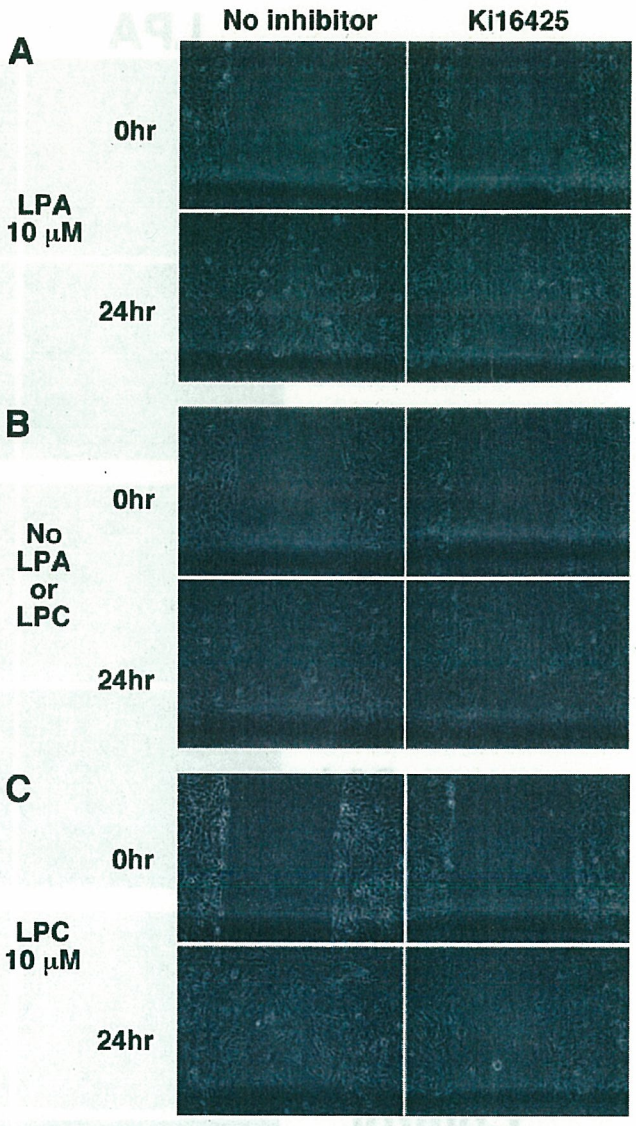

FIGURE 6. **Glioblastoma migrates in response to LPA and LPC in wound healing assay.** A clean wound area was produced on a monolayer of semiconfluent SNB-78 cells, seeded in 12-well plates. The wound was then allowed to heal for 24 h in serum-free media in the presence of LPA (10 μM, *A*) or LPC (10 μM, *C*) or in the absence of exogenous lipids (*B*). Cell morphologies before (0 h) and after (24 h) the treatment are shown in the *upper* and *lower panels*, respectively. The effect of Ki16425 (1 μM) on the cell migration is also shown in the *right panels*.

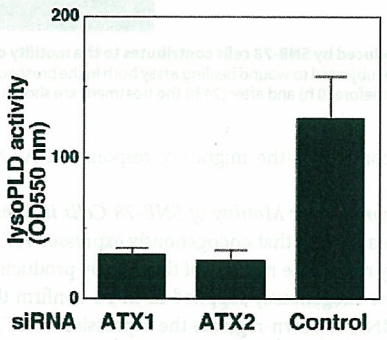

FIGURE 7. **Down-regulation of ATX in SNB-78 cells using siRNA.** One-day postconfluent SNB-78 cells were transfected with ATX (ATX1 and ATX2) or control siRNA duplexes. Forty-eight hours later, down-regulation of ATX in the cell supernatants was analyzed by measuring lysoPLD activity in the cell culture supernatant of the cells.

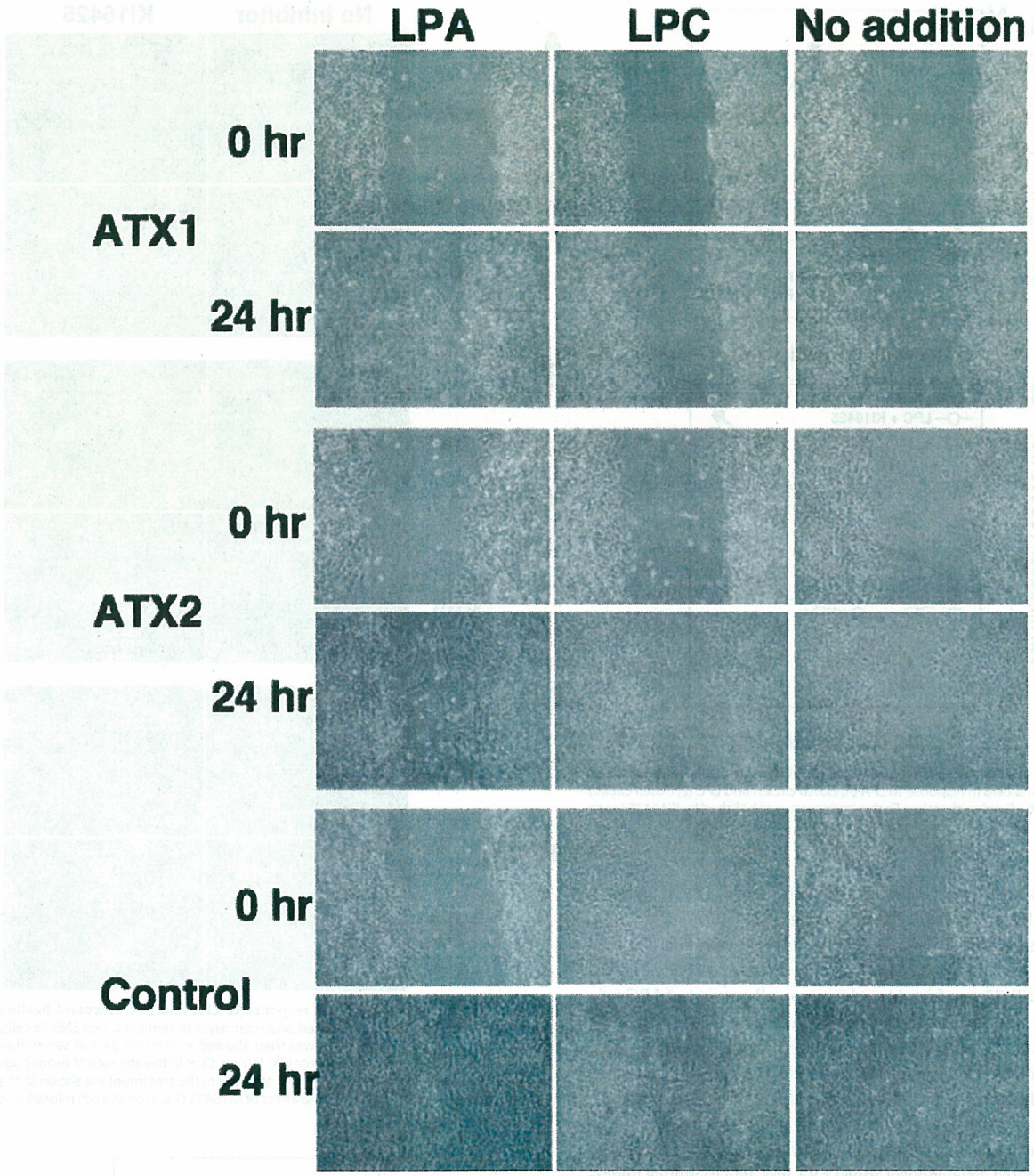

FIGURE 8. **ATX produced by SNB-78 cells contributes to the motility of the cells.** SNB-78 cells were transfected with ATX or control siRNA duplex to suppress ATX level, and after 24 h, the cells were subjected to wound healing assay both in the presence and in the absence of LPC (10 μM) for 24 h. The cells were also treated with LPA (10 μM) as a positive control. Cell morphologies before (0 h) and after (24 h) the treatment are shown in the *upper* and *lower panels*, respectively.

key factor in controlling the migratory response of ATX-expressing cells.

ATX Is Responsible for Motility of SNB-78 Cells in Wound Healing Assay—Our data suggest that endogenously expressed ATX in SNB-78 cells plays a key role in the motility of the cells by producing LPA from endogenously or exogenously supplied LPC. To confirm this hypothesis, we used siRNA to down-regulate the expression of ATX in SNB-78 cells. Confluent SNB-78 cells were transfected with varying amounts of siRNA duplexes using scramble siRNA as a control. As shown in Fig. 7, after 48 h of culture, successful down-regulation of ATX in the cell culture supernatants was confirmed by measuring lysoPLD activity of the culture cell supernatant. We next performed the wound healing assay using the ATX-down-regulated cells. We found that motility of SNB-78 cells was significantly suppressed both in the absence and in the presence of LPC, when the cells were treated with siRNA to suppress ATX expression (Fig. 8). Exogenously added LPA was able to induce migration of ATX-down-regulated cells (Fig. 8), showing that the siRNA-treated cells still retained the migratory activity in response to LPA. Thus, we concluded that ATX contributes to the cell migration of SNB-78 cells in the wound healing assay.

DISCUSSION

GBM is the most malignant brain tumor due to its high invasiveness. In this study, we found that ATX, a cell motility-stimulating factor (4), is overexpressed in GBM tissues and many glioblastoma cell lines. ATX has catalytic activity to produce a potent chemoattractant-like lipid, LPA, and stimulates cell motility through an LPA G-protein-coupled receptor, LPA_1 (14, 21). Interestingly, both GBM tissues and glioblastomas express high levels of LPA_1, and in fact, the glioblastoma, SNB-78, used in this study showed migratory responses not only to LPA but also to LPC (Figs. 5 and 6). In addition, suppression of ATX expression in SNB-78 cells by siRNA resulted in dramatic reduction of migratory response of the cells to LPC but not to LPA (Fig. 8). Furthermore, LPA_1 antagonist, Ki16425, effectively suppressed both LPA- and LPC-induced motility of glioblastoma cells. Thus, the motility of glioblastoma cells appears to depend on ATX and LPA_1. LPA-induced cell motility of glioblastomas was also shown in the previous report by Manning *et al.* (16).

Enhanced ATX expression has been repeatedly demonstrated in various tumors, including non-small cell lung cancer, breast cancer, renal cell cancer, hepatocellular carcinoma, and thyroid cancer (6–12). In breast cancer, ATX expression level strongly correlates with the invasiveness of cancer cells (8). Thus, it is reasonable to assume that ATX expressed by tumor cells is responsible for the motility, and thus, the invasiveness of the cells. However, the spontaneous motility of non-small cell lung cancer cells *in vitro* did not correlate with the levels of ATX mRNA (6), indicating that other factors may influence ATX-induced cell motility. In this study, we used glioblastoma cell lines that endogenously express ATX and cell transformants overexpressing ATX and evaluated ATX, LPA_1, and LPC, a substrate for ATX of lysoPLD activity. Our results show that LPC is a critical factor that regulates ATX-mediated cell motility. We previously showed that LPC is synthesized and released from various tumor cells and that it is a potential substrate for ATX when ATX is added to the cells in the absence of exogenous LPC (14). However, the concentration of cell-derived LPC (~50 nM) is too low to induce full cell motility of SNB-78 cells (Fig. 6). Although a high dose of exogenously added ATX induced cell motility (by converting cell-derived LPC to LPA), the amounts of endogenously expressed ATX in glioblastoma cells and even in ATX-overexpressing glioma cells were insufficient to have an effect on cell motility. We found that the addition of exogenous LPC to the ATX-expressing cells but not ATX-negative cells strongly induced cell motility, although LPA equally promoted the motility of both cell types (Figs. 4–6). Thus, LPC is a chemotactic factor for tumor cells expressing ATX and LPA_1. LPC has previously been shown to act as a chemotactic factor for other cell types, including macrophages (40), monocytes (41), and T-lymphocytes (42). In some cell types, such as macrophages, cell motility appears to be induced by another system (LPC-specific G-protein-coupled receptor, G2A) (43), whereas in other cell types, cell motility appears to be induced by the ATX-LPA_1 system.

In general, the BBB is disrupted in GBM tissue, which leads to exposure of tumor cells to components of plasma that might affect the cell motility of glioblastomas (31, 32). As indicated by Manning *et al.* (16), one such plasma component may be LPA. However, LPA concentration in plasma is quite low (below 50 nM), although in serum, it may be above 1 μM (44, 45). In contrast, LPC concentration in plasma is extremely high (100–300 μM in human and ~500 μM in rats) (35, 44). The concentration of LPC in brain tissue, such as in cerebrospinal fluids, is quite low (several μM level) (46). Thus, when the BBB is disrupted in GBM, it is likely that these tumors are exposed to LPC derived from plasma. LPC is converted to LPA by ATX expressed by glioblastomas, and consequently, LPA_1 is activated, leading to the enhanced cell motility and high invasiveness of GBM (Fig. 9). This idea is supported by the finding that GBM cells travel along blood vessels (47).

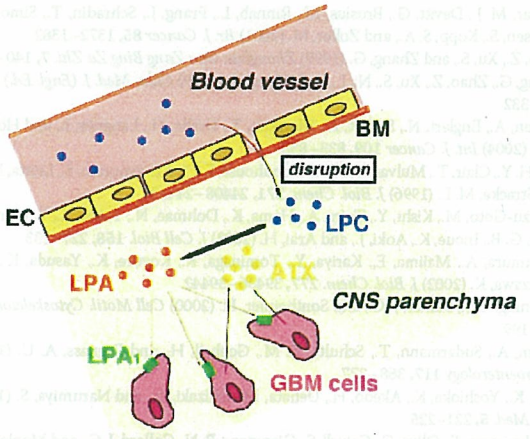

FIGURE 9. **A schematic model showing the effects of ATX, LPA_1, LPA, and LPC on the motility of GBM cells upon the disruption of BBB.** On disruption of BBB, GBM in CNS parenchyma is likely to be exposed to LPC derived from plasma. Then LPC is converted to LPA by ATX expressed by GBM and subsequently activation of LPA_1, leading to the enhanced motility and high invasiveness of GBM. *EC*, endothelial cells; *BM*, basement membrane.

The expression patterns of LPA receptors in the 50 cancer cell lines (Fig. 1) agree with the previous reports on LPA receptor expression. For example, LPA_3 expression is relatively high in cells from ovarian cancer (48) and, markedly, LPA_2 is predominantly expressed in cells derived from colon (37) and thyroid cancer (49). Recently, we also observed similar LPA receptor distribution patterns in human breast cancers (36) in which LPA_2 expression is dramatically enhanced. The present study revealed that LPA_1 is predominantly expressed in GBM cells and tissues. The same is true for ATX. Thus, the expression patterns in cancer cell lines are definitely informative to understand the roles of ATX and LPA receptors in cancer cell biology.

ATX may contribute to cancer cell survival and motility in several ways. In addition to its cell motility-stimulating activity, ATX has a cell proliferation-stimulating activity (14) and an angiogenic factor-like activity that induces new vessel formation by an unknown mechanism (50). GBM is known to induce vascular proliferation, and so ATX might have a role here as well. In summary, our results show that ATX, a potent oncogenic protein, is overexpressed in GBM and stimulates the motility of glioblastomas. Thus, ATX is a potential diagnostic marker for GBM. In addition, ATX, LPA_1 and unidentified LPC-producing enzymes are potential targets for GBM therapy.

REFERENCES

1. Stracke, M. L., Krutzsch, H. C., Unsworth, E. J., Arestad, A., Cioce, V., Schiffmann, E., and Liotta, L. A. (1992) *J. Biol. Chem.* **267,** 2524–2529
2. Goding, J. W., Terkeltaub, R., Maurice, M., Deterre, P., Sali, A., and Belli, S. I. (1998) *Immunol. Rev.* **161,** 11–26
3. Stefan, C., Gijsbers, R., Stalmans, W., and Bollen, M. (1999) *Biochim. Biophys. Acta* **1450,** 45–52
4. Stracke, M. L., Clair, T., and Liotta, L. A. (1997) *Adv. Enzyme Regul.* **37,** 135–144
5. Nam, S. W., Clair, T., Campo, C. K., Lee, H. Y., Liotta, L. A., and Stracke, M. L. (2000) *Oncogene* **19,** 241–247
6. Yang, Y., Mou, L. j., Liu, N., and Tsao, M. S. (1999) *Am. J. Respir. Cell Mol. Biol.* **21,** 216–222
7. Euer, N., Schwirzke, M., Evtimova, V., Burtscher, H., Jarsch, M., Tarin, D., and Weidle, U. H. (2002) *Anticancer Res.* **22,** 733–740
8. Yang, S. Y., Lee, J., Park, C. G., Kim, S., Hong, S., Chung, H. C., Min, S. K., Han, J. W., Lee, H. W., and Lee, H. Y. (2002) *Clin. Exp. Metastasis* **19,** 603–608

9. Stassar, M. J., Devitt, G., Brosius, M., Rinnab, L., Prang, J., Schradin, T., Simon, J., Petersen, S., Kopp, S. A., and Zoller, M. (2001) *Br. J. Cancer* **85,** 1372–1382
10. Zhao, Z., Xu, S., and Zhang, G. (1999) *Zhonghua Gan Zang Bing Za Zhi.* **7,** 140–141
11. Zhang, G., Zhao, Z., Xu, S., Ni, L., and Wang, X. (1999) *Chin. Med. J. (Engl. Ed.)* **112,** 330–332
12. Kehlen, A., Englert, N., Seifert, A., Klonisch, T., Dralle, H., Langner, J., and Hoang, V. C. (2004) *Int. J. Cancer* **109,** 833–838
13. Lee, H. Y., Clair, T., Mulvaney, P. T., Woodhouse, E. C., Aznavoorian, S., Liotta, L. A., and Stracke, M. L. (1996) *J. Biol. Chem.* **271,** 24408–24412
14. Umezu-Goto, M., Kishi, Y., Taira, A., Hama, K., Dohmae, N., Takio, K., Yamori, T., Mills, G. B., Inoue, K., Aoki, J., and Arai, H. (2002) *J. Cell Biol.* **158,** 227–233
15. Tokumura, A., Majima, E., Kariya, Y., Tominaga, K., Kogure, K., Yasuda, K., and Fukuzawa, K. (2002) *J. Biol. Chem.* **277,** 39436–39442
16. Manning, T. J., Parker, J. C., and Sontheimer, H. (2000) *Cell Motil. Cytoskeleton* **45,** 185–199
17. Sturm, A., Sudermann, T., Schulte, K. M., Goebell, H., and Dignass, A. U. (1999) *Gastroenterology* **117,** 368–377
18. Itoh, K., Yoshioka, K., Akedo, H., Uehata, M., Ishizaki, T., and Narumiya, S. (1999) *Nat. Med.* **5,** 221–225
19. Van Leeuwen, F., Olivo, C., Grivell, S., Giepmans, B. N., Collard, J. G., and Moolenaar, W. H. (2003) *J. Biol. Chem.* **278,** 400–406
20. Shida, D., Kitayama, J., Yamaguchi, H., Okaji, Y., Tsuno, N. H., Watanabe, T., Takuwa, Y., and Nagawa, H. (2003) *Cancer Res.* **63,** 1706–1711
21. Hama, K., Aoki, J., Fukaya, M., Kishi, Y., Sakai, T., Suzuki, R., Ohta, H., Yamori, T., Watanabe, M., Chun, J., and Arai, H. (2004) *J. Biol. Chem.* **279,** 17634–17639
22. Yamada, T., Sato, K., Komachi, M., Malchinkhuu, E., Tobo, M., Kimura, T., Kuwabara, A., Yanagita, Y., Ikeya, T., Tanahashi, Y., Ogawa, T., Ohwada, S., Morishita, Y., Ohta, H., Im, D. S., Tamoto, K., Tomura, H., and Okajima, F. (2004) *J. Biol. Chem.* **279,** 6595–6605
23. Tanaka, M., Kishi, Y., Takanezawa, Y., Kakehi, Y., Aoki, J., and Arai, H. (2004) *FEBS Lett.* **571,** 197–204
24. Fang, X., Gaudette, D., Furui, T., Mao, M., Estrella, V., Eder, A., Pustilnik, T., Sasagawa, T., Lapushin, R., Yu, S., Jaffe, R. B., Wiener, J. R., Erickson, J. R., and Mills, G. B. (2000) *Ann. N. Y. Acad. Sci.* **905,** 188–208
25. Fujimaki, T., Matsutani, M., Nakamura, O., Asai, A., Funada, N., Koike, M., Segawa, H., Aritake, K., Fukushima, T., Houjo, S., and *et al.* (1991) *Cancer* **67,** 1629–1634
26. Fujimaki, T. (2000) *Neurol. Med.-Chir. (Tokyo)* **40,** 1–106
27. Burger, P. C., Dubois, P. J., Schold, S. J., Smith, K. J., Odom, G. L., Crafts, D. C., and Giangaspero, F. (1983) *J. Neurosurg.* **58,** 159–169
28. Giese, A., Rief, M. D., Loo, M. A., and Berens, M. E. (1994) *Cancer Res.* **54,** 3897–3904
29. Hauglan, H., Tysnes, B., and Tysnes, O. (1997) *Anticancer Res.* **17,** 1035–1043
30. Westermarck, J., and Khri, V. (1999) *FASEB J.* **13,** 781–792
31. Wolff, M., and Boker, D.-K. (1999) *Clin. Neuropathol.* **8,** 72–78
32. Seitz, R., and Wechsler, W. (1987) *Acta Neuropathol.* **73,** 145–152
33. Yamori, T., Matsunaga, A., Sato, S., Yamazaki, K., Komi, A., Ishizu, K., Mita, I., Edatsugi, H., Matsuba, Y., Takezawa, K., Nakanishi, O., Kohno, H., Nakajima, Y., Komatsu, H., Andoh, T., and Tsuruo, T. (1999) *Cancer Res.* **59,** 4042–4049
34. Niwa, H., Yamamura, K., and Miyazaki, J. (1991) *Gene (Amst.)* **108,** 193–199
35. Kishimoto, T., Soda, Y., Matsuyama, Y., and Mizuno, K. (2002) *Clin. Biochem.* **35,** 411–416
36. Kitayama, J., Shida, D., Sako, A., Ishikawa, M., Hama, K., Aoki, J., Arai, H., and Nagawa, H. (2004) *Breast Cancer Res.* **6,** R640-R646
37. Shida, D., Watanabe, T., Aoki, J., Hama, K., Kitayama, J., Sonoda, H., Kishi, Y., Yamaguchi, H., Sasaki, S., Sako, A., Konishi, T., Arai, H., and Nagawa, H. (2004) *Lab. Investig.* **84,** 1352–1362
38. An, S., Bleu, T., Hallmark, O. G., and Goetzl, E. J. (1998) *J. Biol. Chem.* **273,** 7906–7910
39. Bandoh, K., Aoki, J., Hosono, H., Kobayashi, S., Kobayashi, T., Murakami, M. K., Tsujimoto, M., Arai, H., and Inoue, K. (1999) *J. Biol. Chem.* **274,** 27776–27785
40. Lauber, K., Bohn, E., Krober, S. M., Xiao, Y. J., Blumenthal, S. G., Lindemann, R. K., Marini, P., Wiedig, C., Zobywalski, A., Baksh, S., Xu, Y., Autenrieth, I. B., Schulze, O. K., Belka, C., Stuhler, G., and Wesselborg, S. (2003) *Cell* **113,** 717–730
41. Hoffman, R. D., Kligerman, M., Sundt, T. M., Anderson, N. D., and Shin, H. S. (1982) *Proc. Natl. Acad. Sci. U. S. A.* **79,** 3285–3289
42. Ryborg, A., Deleuran, B., Thestrup-Pedersen, K., and Kragballe, K. (1994) *Arch. Dermatol. Res.* **286,** 462–465
43. Radu, C. G., Yang, L. V., Riedinger, M., Au, M., and Witte, O. N. (2004) *Proc. Natl. Acad. Sci. U. S. A.* **101,** 245–250
44. Aoki, J., Taira, A., Takanezawa, Y., Kishi, Y., Hama, K., Kishimoto, T., Mizuno, K., Saku, K., Taguchi, R., and Arai, H. (2002) *J. Biol. Chem.* **277,** 48737–48744
45. Sano, T., Baker, D. L., Virag, T., Wada, A., Yatomi, Y., Kobayashi, T., Igarashi, Y., and Tigyi, G. J. (2002) *J. Biol. Chem.* **277,** 21197–21206
46. Mulder, C., Wahlund, L. O., Teerlink, T., Blomberg, M., Veerhuis, R., van, K. G., Scheltens, P., and Scheffer, P. G. (2003) *J. Neural Transm.* **110,** 949–955
47. Pedersen, P. H., Edvardsen, K., Garcia-Cabrera, I., Mahesparan, R., Thorsen, J., Mathisen, B., Rosenblum, M. L., and Bjerkvig, R. (1995) *Int. J. Cancer* **62,** 767–771
48. Mills, G. B., Eder, A., Fang, X., Hasegawa, Y., Mao, M., Lu, Y., Tanyi, J., Tabassam, F. H., Wiener, J., Lapushin, R., Yu, S., Parrott, J. A., Compton, T., Tribley, W., Fishman, D., Stack, M. S., Gaudette, D., Jaffe, R., Furui, T., Aoki, J., and Erickson, J. R. (2002) *Cancer Treat. Res.* **107,** 259–283
49. Schulte, K. M., Beyer, A., Kohrer, K., Oberhauser, S., and Roher, H. D. (2001) *Int. J. Cancer* **92,** 249–256
50. Nam, S. W., Clair, T., Kim, Y. S., McMarlin, A., Schiffmann, E., Liotta, L. A., and Stracke, M. L. (2001) *Cancer Res.* **61,** 6938–6944
51. Bligh, E. G., and Dyer, W. J. (1959) *Can. J. BioChem. Physiol.* **37,** 911–917

THE JOURNAL OF BIOLOGICAL CHEMISTRY VOL. 281, NO. 49, pp. 37507–37516, December 8, 2006

Unique and Overlapping Transcriptional Roles of Arylhydrocarbon Receptor Nuclear Translocator (Arnt) and Arnt2 in Xenobiotic and Hypoxic Responses*

Received for publication, July 20, 2006, and in revised form, September 13, 2006 Published, JBC Papers in Press, October 5, 2006, DOI 10.1074/jbc.M606910200

Hiroki Sekine[‡], Junsei Mimura[‡§], Masayuki Yamamoto[‡], and Yoshiaki Fujii-Kuriyama[‡§1]

From the [‡]Center for Tsukuba Advanced Research Alliance and Institute of Basic Medical Sciences, University of Tsukuba, 1-1-1 Tennoudai, Tsukuba 305-8577, Japan and [§]SORST, Japan Science and Technology Agency, 4-1-8 Honcho, Kawaguchi, 332-0012 Japan

Arnt and the homologous Arnt2 share a high degree of sequence similarity and are believed to function as obligate common partners for a number of basic helix-loop-helix (bHLH)-PAS transcription factors including arylhydrocarbon receptor (AhR) and HIFα. Genetic disruption of both Arnt and Arnt2 demonstrated both unique and overlapping functions in response to environmental stimuli and during mouse development. Either stably or transiently expressed Arnt/Arnt2 wild type and various mutants or chimeric constructs in Hepa1-c4 cells exhibit similar levels of hypoxic response element-driven reporter gene expression and the induction of endogenous *Glut-1* through binding with HIFα in response to hypoxia. In contrast, we observed clear functional differences in the ability of Arnt and Arnt2 to induce xenobiotic response element-driven reporter and endogenous *CYP1A1* gene expression. In contrast with Arnt, Arnt2 was practically incapable of interacting with ligand-activated AhR to induce the expression of target genes for xenobiotic-metabolizing enzymes in response to xenobiotics. The differential binding of AhR by Arnt and Arnt2 can be ascribed to a single His/Pro amino acid difference in the PASB region of Arnt and Arnt2, suggesting that the PASB/PASB interaction between bHLH-PAS transcription factors plays a selective role for their specific partner molecule.

Arylhydrocarbon receptor nuclear translocator (Arnt)[2] is a nuclear localized transcription factor that is a canonical member of a transcription factor family consisting of an N-terminal basic helix-loop-helix (bHLH) domain followed by a PAS domain, so named because it is conserved among Per, Arnt, and Sim (1–5). In contrast, the arylhydrocarbon receptor (AhR), a member of the same transcription factor family, associates with an HSP90 complex in the cytoplasm and, upon binding an exogenous inducer such as 3-methylcholanthrene (3MC) or 2,3,7,8-tetrachlorodibenzo-*p*-dioxin (TCDD), translocates from the cytoplasm to the nucleus. Within the nucleus, AhR dissociates from HSP90 and forms a heterodimer with Arnt. The newly formed AhR·Arnt complex binds *cis*-acting DNA enhancer sequences, known as xenobiotic response element (XRE), or dioxin response element (DRE), to enhance the expression of a number of drug-metabolizing enzyme genes including cytochrome P4501A1 (*CYP1A1*) (6). Furthermore, AhR·Arnt signaling is essential for liver and palate development as well as normal reproductive homeostasis, as shown by studies on AhR-deficient mice (7, 8).

Under normoxic conditions, expression of the bHLH-PAS transcription factors hypoxia-inducible factor (HIF)-1α and HIF2α is negatively regulated by the von Hippel-Lindau tumor suppressor protein through the 26 S proteasome (9). However, under hypoxic conditions, HIFα is stabilized and translocates into the nucleus, where it forms a heterodimer with Arnt and binds the hypoxic response element (HRE) leading to the expression of target genes involved in glycolysis, erythropoiesis, and angiogenesis (6). In addition, HIF1α and HIF2α may be involved in normal embryonic development (10–12).

Arnt2, first identified as a homologue with a high degree of sequence similarity to Arnt, undergoes heterodimerization with other bHLH-PAS transcription factors, but unlike the ubiquitously expressed Arnt, Arnt2 expression is restricted to neural tissues and the kidney (13, 14). Arnt2-deficient mice die in the perinatal period and have impaired hypothalamic development (15), but targeted disruption of the Arnt gene leads to embryonic lethality between E9.5 and E10.5 characterized by disrupted placental, hematopoietic and yolk sac vascular development (16–19). When compound heterozygous $Arnt^{2+/-}$ and $Arnt^{+/-}$ mice were mated, all homozygous double mutant mice died before E8.5, and a much smaller number of compound heterozygous $Arnt^{-/-}Arnt^{2+/-}$ or $Arnt^{+/-}$ $Arnt2^{-/-}$ mutant fetuses were found to be alive at E8.5 than expected from Mendelian genetics, suggesting a strong genetic interaction between Arnt2 and Arnt during mouse development (20). Thus, although the expression and functions of Arnt2 and Arnt are not entirely overlapping, there is a strong genetic and functional interaction during development. We wished to deter-

* This work was funded in part by Solution Oriented Research for Science and Technology, Japan Science and Technology Agency and by a grant for Scientific Research from the Ministry of Health, Labor, and Welfare of Japan. The costs of publication of this article were defrayed in part by the payment of page charges. This article must therefore be hereby marked "*advertisement*" in accordance with 18 U.S.C. Section 1734 solely to indicate this fact.

[1] To whom correspondence should be addressed: Center for Tsukuba Advanced Research Alliance, University of Tsukuba, 1-1-1 Tennoudai, Tsukuba, Ibaraki 305-8577 Japan. Tel.: 81-29-853-7323; Fax: 81-29-853-7318; E-mail: ykfujii@tara.tsukuba.ac.jp.

[2] The abbreviations used are: Arnt, arylhydrocarbon receptor nuclear translocator; mArnt, mouse Arnt; 3MC, 3-methylcholanthrene; TCDD, 2,3,7,8-tetrachlorodibenzo-*p*-dioxin; bHLH, basic helix-loop-helix; AhR, arylhydrocarbon receptor; HIF, hypoxia-inducible factor; XRE, xenobiotic response element; HRE, hypoxic response element; E, embryonic day; PBS, phosphate-buffered saline; WT, wild type; aa, amino acid(s).

mine the biochemical and molecular basis for the observed differential roles of Arnt and Arnt2 in physiology and development. Although in our previous report on the transient DNA transfection experiments Arnt2 exhibited some 20% transactivation activity of Arnt with XRE-driven reporter gene (13), stably expressed Arnt2 in transformant cells failed to induce the expression of the XRE-reporter and endogenous *CYP1A1* genes in sharp contrast with studies of Arnt. Interestingly, the differential activity between Arnt and Arnt2 in heterodimer formation with AhR can be ascribed to a single amino acid replacement in the PASB domain.

EXPERIMENTAL PROCEDURES

Plasmids—mArnt and mArnt2 in pBSK were cleaved with NcoI and fused at their N termini with a 3xFLAG tag derived from p3xFLAG-CMV-10 (Sigma). pBSK3xFLAG-Arnt and pBSK3xFLAG-Anrt2 were cleaved with EcoRI and XbaI, and the isolated inserts were blunt-ended and subsequently cloned into XbaI-digested blunt-ended pEFBOS (21) to produce pBOS3xFLAG-Arnt and pBOS3xFLAG-Arnt2. Arnt/Arnt2 chimeras were produced and designated as follows: 3xFLAG-A1(A2TA); 3xFLAG-Arnt N-terminal region (aa 1–465) was connected with the Arnt2 C-terminal region (aa 440–712), 3xFLAG-A2(A1TA); 3xFLAG-Arnt2 N-terminal region (aa 1–439) was connected with the Arnt C-terminal region (aa 466–791), 3xFLAG-A1(A2AB), and 3xFLAG-A2(A1AB); 3xFLAG Arnt or Arnt2 PAS domain was replaced with the Arnt2 or Arnt PAS domain (Arnt-(156–465), Arnt2-(130–439)), respectively (see Fig. 2*A* for summary), 3xFLAG-A1(A2A); 3xFLAG-Arnt PASA domain was replaced with the Arnt2 PASA domain (Arnt-(156–356), Arnt2-(130–330)), respectively (see Fig. 5*A* for summary), 3xFLAG-A1(A2B); 3xFLAG Arnt PASB domain was replaced with the Arnt2 PASB domain (Arnt-(357–465), Arnt2-(331–439)) (see Fig. 5*A* for summary). These cDNA expression vectors were generated using the standard methods and confirmed by sequencing, and the inserts were then cloned into the pBOS vector. pBOS3xFLAG-ArntH378P, pBOS3xFLAG-A1(A2A)H378P, and pBOS-3xFLAG-A1(A2B)P352H were generated by site-directed mutagenesis using the Sculptor *in vitro* mutagenesis system (Amersham Biosciences) with pBOS3xFLAG-Arnt, pBOS3xFLAG-A1(A2A), and pBOS3xFLAG-A1(A2B), as templates, respectively (See Fig. 5*A* for summary).

For construction of pBOSGAL4DBD-Arnt-bHLHPAS-(91–465) and pBOSGAL4DBD-Arnt2-bHLHPAS-(65–439), mArnt-bHLHPAS and mArnt2-bHLHPAS region fragments were produced by PCR, using pBOS3xFLAG-Arnt and pBOS3xFLAG-Arnt2 as templates, and confirmed by sequencing. These fragments were cloned into the pBOSGAL4DBD vector (22). Chimeric constructs were produced and designated as follows: pBOSGAL4DBD-A1A2-bHLHPAS; pBOSGAL-4DBD-Arnt-bHLHPAS N-terminal region (aa 91–257) fused with the Arnt2-bHLHPAS C-terminal region (aa 232–439), pBOSGAL4DBD-A1A2A1-bHLHPAS, A1A1A2-bHLHPAS, A1A2A1–2-bHLHPAS, and A1A1A2–2-bHLHPAS. The sequences of the following regions (aa 258–333, 334–465, 334–397, and 398–465) from pBOSGAL4DBD-Arnt-bHLHPAS were exchanged, respectively, with the corresponding regions of Arnt2-(232–307), -(308–439), -(308–371), and -(372–439). pBOSGAL4DBD-ArntH378P-bHLHPAS was generated by site-directed mutagenesis using pBOSGAL4DBD-Arnt-bHLHPAS as a template.

To produce pBOSVP16AD-mHIF1αΔC, the mHIF1αΔC-(1–613) fragment was generated by PCR using cDNA from Hepa1 RNA as a template and cloned into pGEM-T-Easy vector (Promega). After sequencing, the excised cDNA fragment was inserted into pBOSVP16AD multi-cloning sites (22).

Cell Culture—Hepa1-c4 (an Arnt-defective cell line of Hepa1c1c7 cells (23)), Hepa1, 293T, and HeLa cells were maintained, respectively, in high or low glucose Dulbecco's modified Eagle's medium (Sigma) supplemented with 10% fetal bovine serum (Sigma) and penicillin/streptomycin (Invitrogen) under 5.0% CO_2 at 37 °C.

Reporter Assay—All luciferase assays were performed using the Dual-Luciferase reporter assay system according to the manufacturer's protocol (Promega) with some modifications. Hepa1-c4 cells (2.0×10^4 cells/well) were plated in 24-well plates 24 h prior to transfection. Cells were co-transfected with pXRE4-SV40-Luc (22) or pHRE6-SV40-Luc reporter (24) using 1 ng of *Renilla* luciferase as an internal control and pBOS3xFLAG-Arnt, pBOS3xFLAG-Arnt2, or the chimeric constructs using FuGENE 6 transfection reagent (Roche Applied Science) according to the manufacturer's protocol. All cells were incubated for 24 h at 37 °C after transfection. pXRE4-SV40-Luc-transfected cells were treated with 1 μM 3MC, a potent inducer of XRE-driven transcription, or with Me_2SO and then incubated for an additional 18 h. To measure hypoxia-induced transcription, cells transfected with pHRE6-SV40-Luc were incubated under normoxic or hypoxic (1.0% O_2) conditions for an additional 16 h.

HeLa cells (2.5×10^4 cells/well) were cultured in 24-well plates for 24 h prior to transfection and then were cotransfected with pXRE4-SV40-Luc or pHRE6-SV40-Luc, 1 ng of *Renilla* luciferase as an internal control, effector plasmid (pBOS3x-FLAG-Arnt, pBOS3xFLAG-Arnt2, chimeric or mutant constructs), and partner molecule plasmid (either pBOSmAhR (22) or pBOShHif1α (24)) using Lipofectamine Plus (Invitrogen) according to the manufacturer's protocol. After an additional 24 h of incubation, cells were treated with 3MC or placed under hypoxic condition as described above.

For the Arnt-AhR two-hybrid assay, 293T cells (2.0×10^4 cells/well) were cultured in 24-well plates 24 h prior to transfection and cotransfected with 100 ng of pG3-Luc (22), 0.1 ng of *Renilla* luciferase reporter as an internal control, 10 ng of the bait plasmid (either pBOSGAL4DBD-Arnt, -Arnt2-bHLHPAS, or chimeric or mutant constructs), and 60 ng of prey plasmid (either pBOSVP16AD-mAhRΔC (22) or pBOSVP16AD-mAhRΔBΔC) using Lipofectamine Plus (Invitrogen). For Arnt-HIF1α two-hybrid assay, cultured 293T cells were cotransfected with 100 ng of pG3-Luc (22), 0.1 ng of *Renilla* luciferase reporter as an internal control, 2 ng of the bait plasmid (either pBOSGAL4DBD-mArnt, pBOSGAL4DBD-mArnt2-bHLHPAS, or chimeric and mutants constructs), and 5 ng of pBOSVP16AD-mHIF1αΔC as described above. 3MC and hypoxia treatment were performed as described above.

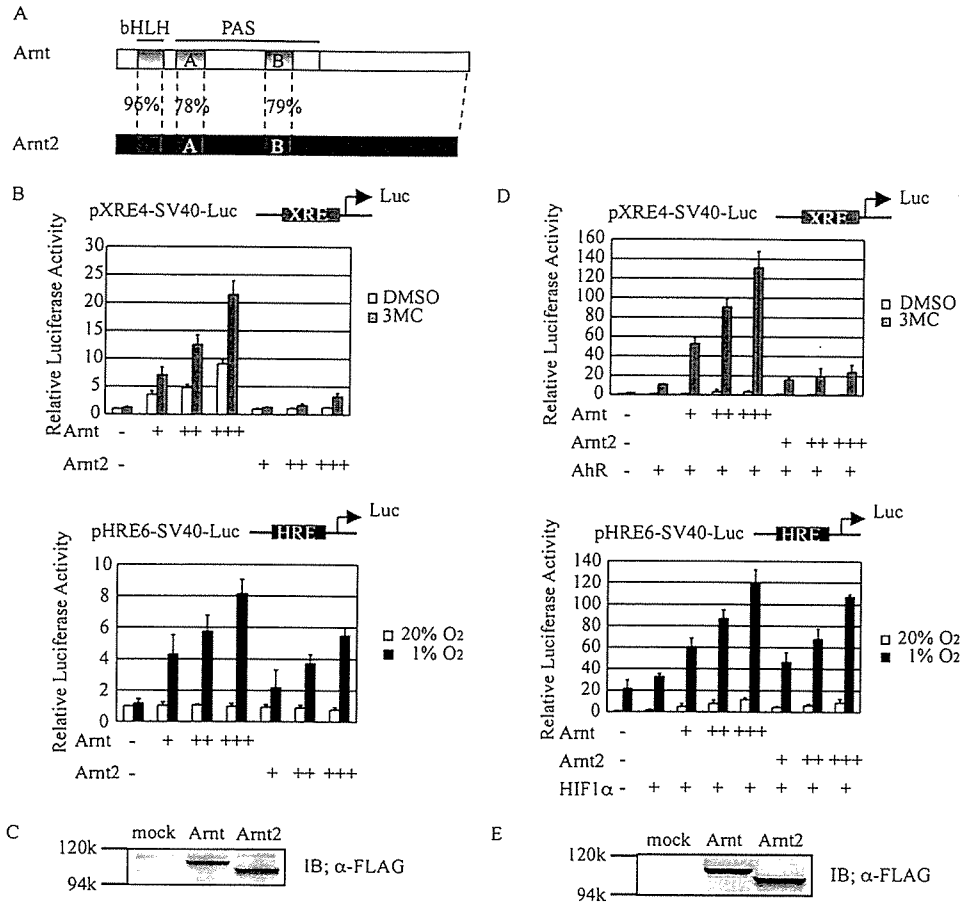

FIGURE 1. **Transcriptional activity of Arnt and Arnt2 on XRE- and HRE-driven reporter genes in Hepa1-c4 and HeLa cells.** *A*, amino acid identities between Arnt and Arnt2. *B*, transcriptional activity of Arnt and Arnt2 in Hepa1-c4 cells. Hepa1-c4 cells were transfected with 100 ng of pXRE4-SV40-Luc and increasing amounts (1, 10, and 100 ng) of 3xFLAG-Arnt or 3xFLAG-Arnt2 expression plasmids, incubated for 24 h, and treated with 1 μM 3MC or Me_2SO (dimethyl sulfoxide (*DMSO*)) for 18 h (*top panel*). For analysis of the hypoxic response, Hepa1-c4 cells were transfected with 100 ng of pHRE6-SV40-Luc and increasing amounts (1, 10, and 100 ng) of 3xFLAG-Arnt or 3xFLAG-Arnt2 expression plasmids. After 24 h of incubation, the cells were treated for 16 h under conditions of normoxia (20% O_2) or hypoxia (1% O_2) (*bottom panel*). The cell extracts were prepared from the treated cells and used for luciferase assays. Values are represented by mean ± S.D. of the results of three independent experiments normalized to *Renilla* luciferase activity used as an internal control. *C*, expression of Arnt and Arnt2 in Hepa1-c4 cells. Hepa1-c4 cells were transfected with 0.5 μg of the indicated expression construct in 6-well plates. The protein levels were evaluated by Western blotting using anti-FLAG antibody. Equal amounts of cell lysates were used for Western blot analysis. The *mock* lane represents cell lysate transfected with empty vector alone. *D*, transcriptional activity of Arnt and Arnt2 in HeLa cells. *Top panel*, XRE-driven reporter activity. HeLa cells were transfected with 10 ng of pXRE4-SV40-Luc, increasing amounts (0.1, 0.5, and 2 ng) of 3xFLAG-Arnt or -Arnt2 expression plasmids, and 10 ng of pBOSmAhR, and the reporter gene expression assays were performed as described in *B*. *Bottom panel*, HRE-driven reporter activity. HeLa cells were transfected with 10 ng of pHRE6-SV40-Luc, increasing amounts (0.1, 0.5, and 2 ng) of 3xFLAG-Arnt or -Arnt2 expression plasmids, and 20 ng of pBOShHIF1α, and the reporter gene expression assays were performed as described in *B*. Values are represented by mean ± S.D. of the results of three independent experiments normalized to *Renilla* luciferase activity used as an internal control. *E*, expression of Arnt and Arnt2 in HeLa cells. HeLa cells were transfected with 10 ng of the indicated expression construct in 6-well plates. *IB*, immunoblot.

Generation of Stable Transformant Cell Lines—Hepa1-c4 cells were cotransfected with pSVneo and effector plasmid (either pBOS3xFLAG-Arnt, pBOS3xFLAG-Arnt2, or pBOS3x-FLAG-ArntH378P). After transfection, the cells were replated and incubated with selection medium containing 0.5 mg/ml Geneticin (Invitrogen).

Western Blot Analysis—Cells were dissolved in SDS sample buffer, and proteins were separated by SDS-PAGE for Western blot analysis. Proteins were then transferred to polyvinylidene difluoride membranes and blocked in 3% skim milk for 30 min. A rabbit anti-Arnt antiserum (25) or anti-FLAG (Sigma), anti-AhR (Biomol), or anti-actin or anti-VP16AD (Santa Cruz Biotechnology) antibodies were used as primary reagents. After being washed three times in TBS (25 mM Tris/HCl (pH 7.5), 150 mM NaCl) containing 0.1% Triton X-100, membranes were incubated with species-specific horseradish peroxidase-conjugated secondary antibody (Zymed Laboratories Inc.). The protein-antibody complexes were visualized by the enhanced chemiluminescence detection system (Amersham Biosciences) according to the recommendations of the manufacturer.

Whole Cell Lysate Preparation for Coimmunoprecipitation—Hepa1-c4 cells stably transfected with pBOS-3xFLAG-Arnt, pBOS3xFLAG-Arnt2, or pBOS3xFLAG-ArntH-378P were incubated with 1 μM 3MC or Me_2SO for 2 h and washed with ice-cold phosphate-buffered saline followed by TBS. The cells were harvested by scraping, centrifuged at 5,000 rpm at 4 °C for 5 min, and suspended in TBS containing 1 mM $CaCl_2$, 1% Triton X-100, and protease inhibitor mixture (Roche Applied Science). The cells were vortexed and placed on ice for 5 min. The samples were then centrifuged at 15,000 rpm for 5 min at 4 °C, and the supernatants were reserved as whole cell lysates.

Coimmunoprecipitation Assay—The prepared whole cell lysate (200 μl) was added to 200 μl TBS with 1 mM $CaCl_2$ and protease inhibitor mixture and incubated with anti-FLAG antibody for 1 h at 4 °C. The reaction mixture was supplemented with 15 μl of protein A-agarose beads (Amersham Biosciences). After incubating for an additional 1 h at 4 °C, the beads were washed three times with TBS and resuspended in SDS sample buffer. The coimmunoprecipitated proteins were resolved by SDS-PAGE, and Western blot analysis was performed.

Immunohistochemistry—Hepa1-c4 cells stably transfected with pBOS3xFLAG-Arnt, pBOS3xFLAG-Arnt2, or pBOS3x-FLAG-ArntH378P were washed, fixed in 4% paraformaldehyde at room temperature for 10 min, and treated with cold acetone for 1 min on ice. After washing with PBS, the cells were incubated with 3% skim milk for 1 h at room temperature and treated with 10 μg/ml mouse anti-FLAG antibody for 16 h at 4 °C. After washing with PBS, the cells were subsequently

treated with biotinylated anti-mouse IgG antibody (Vector) for 3 h at 4 °C, washed with PBS, and treated with streptavidin-Alexa Fluor 488 (Invitrogen) and Hoechst solution (Dojindo) for 30 min at room temperature. After washing with PBS, a drop of fluorescent mounting medium (Dako) was placed on the cells, which were then examined by fluorescence microscopy.

Real-time PCR—Total RNA samples were prepared from the treated cells using Isogen (Nippon Gene) as described. First-strand cDNA was synthesized from 1 μg of total RNA using SuperScript reverse transcriptase (Invitrogen). Real-time PCR was performed in triplicate for each sample with the ABI Prism 7700 sequence detector (PE Applied Biosystems) using primers designed against mouse *GLUT1* (26) and *CYP1A1* (primer sequences GGTACAGAGAAAGATCCAGGAGGA and CGAAGGATGAATGCCGGAAGGTCT and probe sequence 6-FAM-CTAGACACAGTGATTGGCAGAGATCGGCA-TAMRA) or rRNA genes (PE Applied Biosystems).

RESULTS

Comparison between Transcription Activities of Arnt and Arnt2 for Expression of the XRE- and HRE-driven Reporter Genes—It has been reported that the bHLH and PAS domains of Arnt and Arnt2 are very similar and mediate homo- and heterodimerization (Fig. 1*A*), but Arnt2 showed only 20% transcription activity of Arnt in the expression of the XRE-driven reporter gene (13).

To clarify whether the low transcription activity of Arnt2 for the expression of the XRE reporter gene is because of a low level of expression of Arnt2 or a low affinity of Arnt2 to AhR as compared with Arnt, we investigated the transcription activity of the XRE- and HRE-driven reporter genes by Arnt2 and Arnt in a dose-dependent manner using the transient transfection assay. In an experiment using either Hepa1-c4 or HeLa cells (the same result was obtained with NIH3T3 cells, data not shown), a highly inducible expression of the XRE-driven reporter gene was observed by Arnt in response to 3MC. In marked contrast, Arnt2 exhibited only a low level of inducible expression of the reporter gene even at the highest dose (Fig. 1, *B* and *D*). On the other hand, the HRE-driven reporter gene was induced similarly by Arnt and Arnt2 in response to hypoxia. Taken together with the results that Arnt and Arnt2 were similarly expressed at a protein level as shown in Fig. 1, *C* and *E*, all of these results suggest that Arnt2 is much less efficient than Arnt in conjunction with AhR for the inducible expression of the XRE reporter gene, whereas both Arnt and Arnt2 work equally well with HIFα to regulate the HRE reporter gene expression.

PAS Domain Is Responsible for Differential Activities between Arnt and Arnt2 for XRE-driven Reporter Gene Expression—We were interested in the molecular mechanisms responsible for the differences in transcriptional activity between Arnt and Arnt2. To investigate which part of the Arnt and Arnt2 molecules is responsible for the differential activity, we divided Arnt and Arnt2 into three parts based on the N-terminal bHLH, PAS, and C-terminal activation domains and generated several chimeric constructs by swapping the respective domains for Arnt and Arnt2 (Fig. 2*A*). As shown in the *upper panel* of Fig. 2*B* (*column 1 versus 3*), the luciferase activity is the same in cells

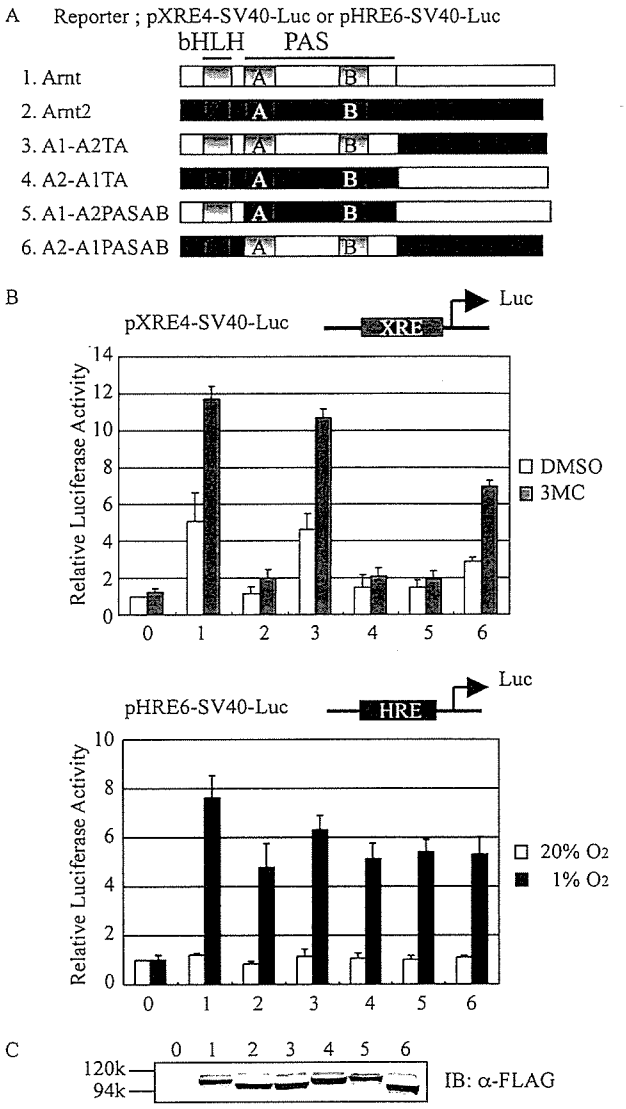

FIGURE 2. **Transcriptional activity of Arnt/Arnt2 chimeric proteins on XRE- and HRE-driven reporter genes in Hepa1-c4 cells.** *A*, Arnt and Arnt2 structures and their domain-swapping constructs. *B*, transcriptional activity of Arnt/Arnt2 chimeric constructs. Hepa1-c4 cells transfected with 100 ng of pXRE4-SV40-Luc and 10 ng of the indicated Arnt/Arnt2 chimeric constructs were incubated for 24 h and then treated with 1 μM 3MC or Me_2SO (dimethyl sulfoxide (*DMSO*)) for 18 h (*top panel*). For analysis of the hypoxic response, Hepa1-c4 cells were transfected with 100 ng of pHRE6-SV40-Luc and 10 ng of the Arnt/Arnt2 chimeric constructs. After 2 h of incubation, the cells were treated for 16 h under normoxia or hypoxia (1% O_2) (*bottom panel*). The cell extracts were prepared from the treated cells and used for luciferase assays. Values are represented by mean ± S.D. of the results of three independent experiments normalized to *Renilla* luciferase activity used as an internal control. *C*, expression of Arnt, Arnt2, and chimeric constructs. The cells were transfected with 50 ng of the indicated expression construct in 6-well plates. The protein levels of all constructs were evaluated by Western blotting using anti-FLAG antibody. Equal amounts of cell lysates were used for Western blot analysis. *Columns* in *B* and *C*: *0*, pBOS; *1*, pBOS3xFLAG-Arnt; *2*, pBOS3xFLAG-Arnt2; *3*, pBOS3xFLAG-A1(A2TA); *4*, pBOS3xFLAG-A2(A1TA); *5*, pBOS3xFLAG-A1(A2AB); *6*, pBOS3xFLAG-A2(A1AB). *IB*, immunoblot.

expressing WT Arnt and a chimera composed of the N-terminal bHLH and PAS domains of Arnt and the C-terminal region of Arnt2. In contrast, a chimera composed of the bHLH and C-terminal domains of Arnt and the PAS domain of Arnt2 activates only a low level of luciferase expression, as observed with WT Arnt2 for the expression of XRE-driven reporter gene (Fig.

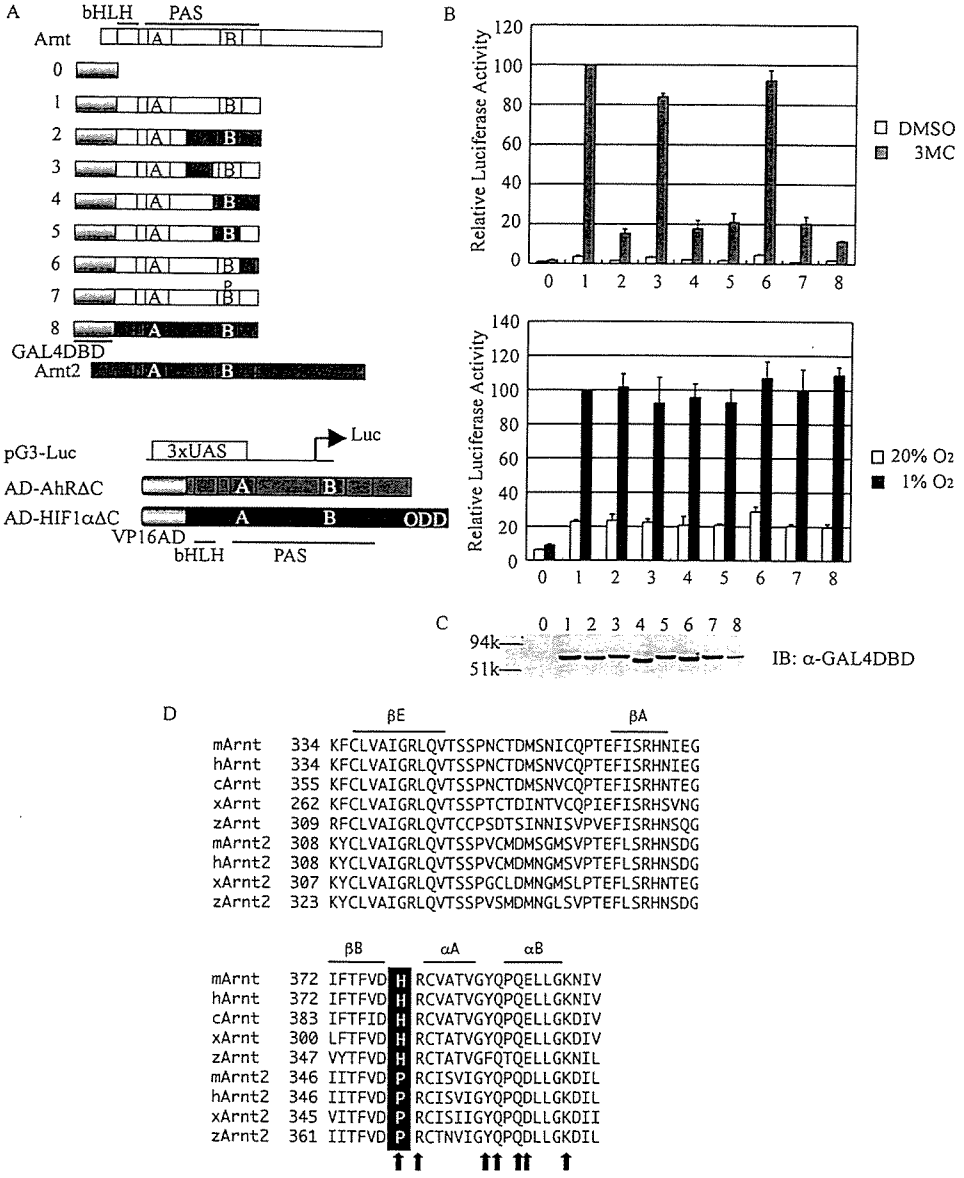

FIGURE 3. **Two-hybrid analysis of transcriptional activities of Arnt and Arnt2 and their chimeric and mutant derivatives.** *A*, constructs of bait proteins of Arnt and Arnt2, their chimeras and mutant, and prey molecules of AhR and HIF1α. *B*, transcriptional activity of various Arnt/Arnt2-bHLHPAS chimeric proteins in the two-hybrid system. 293T cells were transfected with pG3-Luc, the indicated Arnt/Arnt2 construct, and pBOSVP16AD-mAhRΔC (*AD-AhRΔC*) or pBOSVP16AD-mHIF1αΔC (*AD-HIF1αΔC*) (see "Experimental Procedures"). The transfected cells were treated as described in the legend to Fig. 1*B*. *Top panel*, relative luciferase activities induced by 3MC treatment. *Bottom panel*, relative luciferase activities induced by hypoxic treatment. Values are represented by mean ± S.D. of the results of three independent experiments normalized to *Renilla* luciferase activity used as internal control. *DMSO*, dimethyl sulfoxide (Me_2SO). *C*, expression of the bait proteins. The cells were transfected with 50 ng of the indicated expression construct in 6-well plates. Protein levels of all constructs were evaluated by Western blot analysis using α-GAL4DBD antibody. The cells were homogenized, and supernatants were subjected to SDS-PAGE for Western blot analysis (*IB*, immunoblot). *Columns*: *0*, pBOSGAL4DBD; *1*, pBOSGAL4DBD-Arnt-bHLHPAS; *2*, pBOSGAL4DBD-Arnt2-bHLHPAS; *3*, pBOSGAL4DBD-A1A2-bHLHPAS; *4*, pBOSGAL4DBD-A1A2A1–1-bHLHPAS; *5*, pBOSGAL4DBD-A1A1A2–1-bHLHPAS; *6*, pBOSGAL4DBD-A1A2A1–2-bHLHPAS; *7*, pBOSGAL4DBD-A1A1A2–2-bHLHPAS; *8*, pBOSGAL4DBD-ArntH378P-bHLHPAS (see "Experimental Procedures"). The full activity of *column 1* was taken as a standard to calculate relative activities. *D*, amino acid sequences of a part of PASB region of Arnt and Arnt2 responsible for differential transcriptional activities in association with AhR. Predicted exposed side chains of amino acids (27) are indicated by *arrows*. *m*, mouse; *h*, human; *c*, chicken; *x*, *Xenopus*; *z*, zebrafish.

2*B*, *upper panel*, *columns 2* and *5*). Thus, it is not the highly variable C-terminal domain but the PAS domain that is responsible for the differences in XRE-driven luciferase expression. In contrast, any combination of Arnt and Arnt2 domains was able to activate luciferase expression to the same extent in response to hypoxia. Taken together, these results suggest that only the PAS domain of Arnt is capable of efficient heterodimerization with AhR to activate the XRE, but HIFα interacted equally with the PAS domains of Arnt and Arnt2 leading to HRE-mediated transcription.

Interaction of the PAS Domains of Arnt or Arnt2 with Those of AhR and HIF1α—To further investigate the interaction of the PAS domains of Arnt and Arnt2 with AhR, we used a mammalian two-hybrid system. Arnt/Arnt2 bHLH-PAS chimeric constructs fused with the GAL4DBD were used as bait, and AhRΔC or HIF1αΔC fused with the VP16 activation domain were used as preys (Fig. 3*A*). Replacement of only a small portion of the PASB domain of Arnt with that of Arnt2 almost completely abrogated 3MC-induced luciferase expression (Fig. 3*B*, *upper panel*, *columns 2*, *4*, and *5 versus 1*, *3*, and *6*). All constructs were equally expressed except for a slightly lower expression of construction 8 (Fig. 3*C*). Taken together, these data indicate that the critical region for determining the differential interaction of Arnt and Arnt2 with AhR covers the sequence of amino acids 334–397 of Arnt and 308–371 of Arnt2. This region is predicted to form the N-terminal cap and a part of the PAS core of the PASB fold and is thought to be solvent-exposed, forming an interface to interact with partner proteins (27). In this region there are seven amino acids with side chains that are predicted to be solvent-exposed (27) (indicated by *arrows* in Fig. 3*D*), and six are conserved or conservative amino acid replacements between Arnt and Arnt2. Only the replacement of His with Pro was considered to be significant for the functional difference between Arnt and Arnt2. These amino acids, His and Pro, are conserved, respectively, in Arnt and Arnt2 of various animal species (Fig. 3*D*). When we generated a His-to-Pro point mutation in Arnt, this construct was not able to interact efficiently with AhR to activate luciferase expression in response to 3MC (Fig. 3*B*, *upper panel*, *column 7*). On the other hand, all chimeric constructs, WT Arnt and Arnt2, and